Bilateral Teleoperation of Groups of Mobile Robots With Time-Varying Topology

Antonio Franchi, *Member, IEEE*, Cristian Secchi, *Member, IEEE*, Hyoung Il Son, *Member, IEEE*, Heinrich H. Bülthoff, *Member, IEEE*, and Paolo Robuffo Giordano, *Member, IEEE*

***Abstract*—In this paper, a novel decentralized control strategy for bilaterally teleoperating heterogeneous groups of mobile robots from different domains (aerial, ground, marine, and underwater) is proposed. By using a decentralized control architecture, the group of robots, which is treated as the *slave side*, is made able to navigate in a cluttered environment while avoiding obstacles, interrobot collisions, and following the human motion commands. Simultaneously, the human operator acting on the master side is provided with a suitable force feedback informative of the group response and of the interaction with the surrounding environment. Using passivity-based techniques, we allow the behavior of the group to be as flexible as possible with arbitrary split and join events (e.g., due to interrobot visibility/packet losses or specific task requirements) while guaranteeing the stability of the system. We provide a rigorous analysis of the system stability and steady-state characteristics and validate performance through human/hardware-in-the-loop simulations by considering a heterogeneous fleet of unmanned aerial vehicles (UAVs) and unmanned ground vehicles as a case study. Finally, we also provide an experimental validation with four quadrotor UAVs.**

***Index Terms*—Decentralized control, distributed algorithms, distributed robot systems, haptics, mobile agents, multirobot systems, networked robots, passivity-based control, teleoperation of mobile robots, telerobotics.**

I. Introduction

FOR several applications such as surveillance of large perimeters, search and rescue in disaster regions, and exploration of wide or unaccessible areas, the use of a group of simple robots rather than a single complex robot has proven to be very effective, and the problem of coordinating a group of agents has received a lot of attention from the robotics and control community over the past decade (see [1] for a survey). Indeed, such a fruitful interplay has resulted in significant advances in the mathematical formalization, theoretical analysis, and actual realization of complex multirobot systems for diverse applications, such as exploration [2], coverage [3], and cooperative transportation [4]. Nevertheless, when the tasks become extremely complex and high-level cognitive-based decisions are required online, complete autonomy is still far from being reached. In this context, teleoperation systems, where a human operator commands a remote robot through a local interface, can be used to exploit human's intelligence.

In this paper, we study the problem of establishing a *bilateral* teleoperation system for remotely controlling, in a decentralized way, the motion of a heterogeneous group of mobile robots, such as aerial, ground, space, naval, or underwater vehicles. Indeed, the fundamental problem addressed in this study consists of establishing a bilateral teleoperation channel for remote *navigation* purposes, i.e., a necessary premise for any other specific objective, such as teleexploration, teletransport, or telemanipulation. In our envisaged teleoperation system, the remote mobile robots (the *slave side* from now on) should possess some minimum level of local autonomy and act as a *group*, e.g., by maintaining some desired interdistances and avoiding collisions by means of decentralized controllers. At the same time, the human operator, acting on the *master device*, should be in control of the overall group motion and receive, through haptic feedback, suitable cues informative enough of the remote robot/environment state. On top of this remote navigation layer, the group should still be allowed to perform additional local tasks by exploiting the internal slave side redundancy with respect to the master device commands.

Bilateral teleoperation of (multiple) mobile robots presents several differences with respect to conventional teleoperation systems: First, there exists a structural *kinematic dissimilarity* between master and slave sides, i.e., the master possesses a limited workspace, while the slave an unbounded one. Second, in a typical scenario, there is no physical contact with the environment since this would represent a dangerous situation (e.g., a crash) for the robots. Finally, the slave side possesses large motion redundancy with respect to the master side because of the gap between the degrees of freedom (DOFs) of the master (usually in the range of 3–6), and the DOFs of the slave (in the range of $6N$ for N robots, when considered as rigid bodies). A proper design of a multirobot slave side must also cope with the typical requirements of *decentralized sensing and control* for

Manuscript received October 10, 2011; revised February 23, 2012; accepted April 17, 2012. Date of publication May 14, 2012; date of current version September 28, 2012. This paper was recommended for publication by Associate Editor E. Guglielmelli and Editor W. K. Chung upon evaluation of the reviewers comments. This work was supported in part by the World Class University program funded by the Ministry of Education, Science, and Technology through the National Research Foundation of Korea under Grant R31-10008.

A. Franchi, H. I. Son, and P. R. Giordano are with the Max Planck Institute for Biological Cybernetics, 72076 Tübingen, Germany (e-mail: antonio.franchi@tuebingen.mpg.de; hyoungil.son@tuebingen.mpg.de; prg@tuebingen.mpg.de).

C. Secchi is with the Department of Science and Methods of Engineering, University of Modena and Reggio Emilia, 42122 Reggio Emilia, Italy (e-mail: cristian.secchi@unimore.it).

H. H. Bülthoff is with the Max Planck Institute for Biological Cybernetics, 72076 Tübingen, Germany, and also with the Department of Brain and Cognitive Engineering, Korea University, Seoul 136-713, Korea (e-mail: hhb@tuebingen.mpg.de).

This paper has supplementary downloadable material available at http://ieeexplore.ieee.org. provided by the author. The material includes three videos.

Color versions of one or more of the figures in this paper are available online at http://ieeexplore.ieee.org.

Digital Object Identifier 10.1109/TRO.2012.2196304

guaranteeing robustness to failures, achieving actual feasibility, and ensuring low computational load: Roughly speaking, one should avoid the presence of any central sensing, communication, or control unit in the network [1], [5]. Finally, the design of a navigation-oriented teleoperation should allow for the possibility of adding extra tasks independent of the main navigation command received from the human operator. Therefore, stability with respect to time-varying interaction topology within the slave side network should also be granted.

A. Contribution and Relation to Previous Work

A lot of interest is, recently, arising in the robotics community in the bilateral teleoperation of mobile robots (see, for instance, [6]–[8]), where the haptic teleoperation of a *single* mobile robot is considered. In fact, it has been widely proven that the use of a force information allows us to obtain superior performance with respect to the case where no haptic feedback is present (see, e.g., [9]–[12]).

In [13], a conventional multimaster/multislave teleoperation system with no delay is developed and a centralized strategy to control the cooperative behavior of the robots is proposed. In [14] and [15], two approaches to control multiple ground robots through a master device are presented, while in [16], an impedance controller for teleoperating a group of slaves in a leader–follower modality is proposed. Finally, in [17], a bilateral control strategy that allows us to coordinate the motion between the master and the slaves under arbitrary time delay is proposed, while in [18], a related (still passivity based) work that considers fixed topology and deformable but fixed shape is also presented. The main limitations of these approaches are the centralization (every robot needs to communicate with the master and/or with all the other robots) and the rigidity of the fleet which is not allowed, for example, to actively reshape the formation or to vary its topology online because of (arbitrary) internal decisions. Moreover, some of the cited works do not address the master/slave kinematic dissimilarity and consider a standard position–position teleoperation architecture which is not particularly suited for a bilateral teleoperation of *mobile robots*.

Many existing leader–follower concepts could be seen as examples of *unilateral* teleoperation of multiple mobile robots (e.g., see [5] and [19]). Nevertheless, *bilateral* teleoperation does not constitute a straightforward extension because of the additional coupling between the motion of the slave and the forces applied to the master device. Finally, similarly to our work, in [20], the possibility of splitting or joining the formation for double-integrator agents is also considered. However, the authors considered the possibility of splits and joins *only* for excessive interrobot distances: From the slave-side stability point of view, this is a quite simplified situation with respect to the case considered in this study where split and join decisions can be taken *at any time* and because of *any internal criterium*; see Remark 4 in Section II-A for more details.

To the best of our knowledge, this paper is the first attempt in proposing a framework that is able to address most of the aforementioned points by implementing a bilateral teleoperation system for remotely controlling a group of robots in a highly flexible and decentralized way. The theoretical foundation on top of which the paper is built is passivity-based control: On one side, passivity theory is exploited to guarantee a stable behavior of the slave group *per se* despite of autonomous maneuvers, time-varying fleet topology, and interaction with remote obstacles in a clean and powerful manner. On the other side, passivity theory is also instrumental for characterizing the stability of the "feedback interconnection" among the environment/slave side/master side/human–operator as classically done in many previous teleoperation works [21].

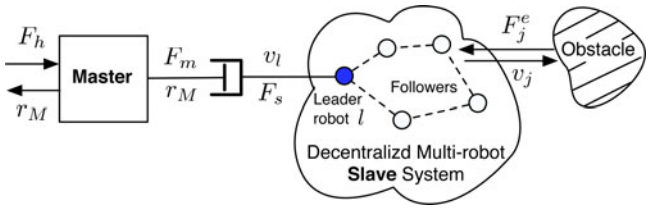

Fig. 1. Overall teleoperation system. From left to right, F_h is the human operator force applied to the master device; r_M is the velocity-like quantity which is almost proportional to the position of the haptic device; F_m is the control force applied to the master in order to provide haptic feedback; v_l is the velocity of the leader; and F_s is the force applied to the leader to make it follow the desired velocity; finally, v_j is the velocity of a generic jth robot, and F_j^{env} is its interaction force with the external environment (obstacles).

The foundations of this approach, which are presented in [22], have been extended in this paper by adding the steady-state analysis, improving the presentation, motivations, theory, and reference to related works, performing more thorough human/hardware-in-the-loop (HHL) simulations, and adding an experiment with a group of four real quadrotor unmanned aerial vehicles (UAVs).

This paper is organized as follows. After presenting the architecture in Section II, Section II-A introduces one of the main contributions of this paper, i.e., a passivity-based modeling of the group of mobile robots and its interaction with the environment. Then, Sections II-B and C describe the master-device model and the master/slave passive interconnection, respectively. Section III formally characterizes the steady-state regime. Finally, HHL simulations using UAVs (quadrotors) and unmanned ground vehicles (UGVs) (differentially driven wheeled robots) are reported in Section IV, as well as experiments obtained with four quadrotor UAVs. Section V concludes this paper and discusses future research directions.

II. Teleoperation System

For the reader's convenience, we will, informally, summarize the architecture of our teleoperation system which will be then rigorously detailed in the next Sections II-A, B, and C. In our scheme, which is depicted Fig. 1, the slave side consists of a group of N agents among which a *leader* is chosen (denoted by the subscript l). The motion of an agent depends on the motion of the locally surrounding agents and obstacles by means of the action of *nonlinear elastic-like couplings*. The leader is a special agent that is also subject to the master control represented by the additional external force F_s. The remaining agents (not controlled by the master) are referred to as *followers*. The

spring coupling between a pair of agents can be broken and/or reestablished at any time. This way, we ensure high flexibility with respect to possible additional tasks, and adequate maneuverability within cluttered environments as the group shape does not result overly constrained. The design and stability analysis of the slave side is thoroughly illustrated in Section II-A and represents a major contribution of this paper.

The velocity-like quantity r_M, (almost) which is proportional to the position of the master device, acts as velocity setpoint for the leader at the slave side thanks to the master/slave coupling force F_s (as explained in Section II-C). This allows us to address the aforementioned master–slave kinematic dissimilarity. Conversely, the mismatch between r_M and the actual leader velocity v_l is transformed into the force F_m at the master side, in order to transmit to the user a feeling of the remote side (see Section II-B). This force will be shown in Section III to carry information about the total number and velocity of agents in the group, and about the interaction with the surrounding environment because of the leader-follower mutual influence.

Passivity will be the leitmotif throughout the whole design and analysis phase. In fact, in order to ensure the stability of the system, our primary goal will be to design the master and slave side as passive systems joined by a passive interconnection. This way, the bilateral teleoperation system will be characterized by a stable behavior in case of interaction with passive environments and passive human users. The choice of relying on the passivity framework is motivated by the following reasons. 1) In classical bilateral teleoperation settings, passivity is a well-established tool to prove stability of the human/master/slave/environment interconnection (see [21] and [23] for a survey); 2) because of the flexible behavior that will be described in Section II-A, the slave side behaves as a switching system. Passivity provides a powerful and elegant tool to enforce its stability under arbitrary switching (see `PassiveJoin` procedure in Section II-A), while, if not using passivity, one should *still* design other strategies to guarantee stability of the slave-side switching dynamics; 3) finally, providing a strategy that could make the slave side stable but *not* passive would nullify the benefits discussed in point 1. Indeed, in this case, one should explicitly prove the stability of the master/slave feedback interconnection rather than exploiting the well-known result of stable interconnection of a (passive) master with a (passive) slave.

Finally, note that the leader can be any robot in communication with the master side—the only requirement is that such a robot does exist at all times. Nevertheless, any specific strategy to choose the leader robot can also be adopted depending on the particular application or task. For instance, the authors in [24] illustrate a way to choose a leader by maximizing the tracking performance of the slave.

A. Slave Side

The slave side consists of a group of N robots coupled together. In this section, we detail a control strategy to obtain a flexible cohesive behavior of the group (i.e., allowing arbitrary split and join) and, at the same time, to avoid interrobot and obstacle collisions.

Every agent is modeled as a floating mass in $\mathbb{R}^3$, i.e., an element storing kinetic energy

$$\begin{cases} \dot{p}_i = F_i^a + F_i^e - B_i M_i^{-1} p_i \\ v_i = \dfrac{\partial \mathcal{K}_i}{\partial p_i} = M_i^{-1} p_i \end{cases} \qquad i = 1, \ldots, N \qquad (1)$$

where $p_i \in \mathbb{R}^3$ and $M_i \in \mathbb{R}^{3\times 3}$ are the momentum and (symmetric positive definite) inertia matrix of agent i, respectively, $\mathcal{K}_i = \frac{1}{2} p_i^T M_i^{-1} p_i$ is the kinetic energy stored by the agent during its motion, and $B_i \in \mathbb{R}^{3\times 3}$ is a positive-definite matrix representing an artificial damping added to asymptotically stabilize the behavior of the agent[1]. Force $F_i^a \in \mathbb{R}^3$ represents the interaction of agent i with the other agents and will be designed in the following, while $F_i^e \in \mathbb{R}^3$ represents the interaction of agent i with the "external world," i.e., the environment (obstacles) and the master side through the teleoperation channel (see Section II-C). Finally, $v_i \in \mathbb{R}^3$ is the velocity of the agent, and $x_i \in \mathbb{R}^3$ its position, with $\dot{x}_i = v_i$.

Note that terms M_i allow us to model different inertial properties depending on the direction of motion (e.g., a quadrotor whose vertical dynamics is usually faster than the horizontal one). Furthermore, we can enforce heterogeneity in the group by providing different inertial characteristics $M_1, \ldots, M_N$ and fluid resistances $B_1, \ldots, B_N$ (e.g., aerodynamic versus hydrodynamic drag).

Remark 1: Depending on the context, (1) can be easily recast in $\mathbb{R}^2$ to, e.g., model ground or naval vehicles by properly including those reaction forces arising from the presence of geometrical constraints (e.g., when motion is bound to a planar surface). We also assume that the robots under consideration are endowed with a controller that is able to track the smooth Cartesian trajectory generated by (1) with small/negligible tracking errors. This is the case, for example, of all the systems with a Cartesian flat output [25], i.e., a point in $\mathbb{R}^3$ that algebraically defines, with its derivatives, the state and the control inputs of the system. Many mobile robots, including the usual nonholonomic ground robots, exhibit this property: For instance, the authors in [26] give a nonexhaustive list of differentially flat mechanical systems such as nonholonomic vehicles or submarines. However, the description of particular trajectory tracking controllers is outside the scope of this paper, e.g., see [27], where a related control strategy for a class of UAVs is discussed.[2]

The following definition will be used later on to define a suitable interaction graph for the group.

Definition 1 (Neighboring Agents): Let $d_{ij} = \|x_i - x_j\|$ be the interdistance among agents i and j, and $\sigma_{ij}(t) : \mathbb{R} \to \{0, 1\}$, $i \neq j$, represent a time-varying Boolean condition satisfying *at least* the following requirements.

1) $\sigma_{ij}(t) = 0$, if $d_{ij} > D \in \mathbb{R}^+$.
2) $\sigma_{ij}(t) = \sigma_{ji}(t)$.

[1] This can also represent typical physical phenomena, e.g., wind/atmosphere drag for UAVs, or hydrodynamic drag for underwater robots.

[2] Alternatively, one could track the flow of (1) with a feedback-linearizable Cartesian output of the robotic system under consideration (e.g., a point off the mid-axle position in differentially driven ground robots). This technique is exploited in [28].

Then, two agents i and j are defined as being neighbors if and only if $\sigma_{ij}(t) = 1$. Furthermore, two agents i and j are said to join if they become neighbors ($\sigma_{ij} = 0 \rightarrow \sigma_{ij} = 1$) and, conversely, are said to split if they become nonneighbors ($\sigma_{ij} = 1 \rightarrow \sigma_{ij} = 0$).

This neighboring definition is purposely stated in a very general form in order to account for any additional task requirement independent of the main navigation command. In this sense, item 1) is meant to model a generic limited range capability of onboard sensors and/or communication complexity of the robot network: Whatever the task at hand, two agents are never allowed to interact if their interdistance overcomes a certain threshold D. However, Definition 1 also leaves the possibility for a $\sigma_{ij}(t) = 0$ even though $d_{ij} \leq D$. This captures our intention of admitting the presence of additional subtasks or constraints the agents may be subject to during their motion. For instance, in our teleoperation framework, the fleet could decide to separate in different logical subgroups in order to accomplish different objectives, but the separation decision could take place when the interdistances are less than D. Similarly, the agents could be equipped with sensors not always able to provide their mutual position even if $d_{ij} < D$ (e.g., visibility sensors such as cameras affected by occlusions, or wireless communication undergoing temporary packet losses), resulting in unwanted but unavoidable disconnections with their neighbors. Nevertheless, when two agents are actually interacting, we also require that they keep some preferred interdistance in order to avoid collisions and to achieve a cohesive behavior of the fleet. Finally, item 2) represents the fact that we aim for a *symmetric* neighboring condition: Two agents always agree on their interaction state.

According to Definition 1, we then denote with $\mathcal{N}_i$ the set of neighbors of i. Since the relationship is symmetrical, $j \in \mathcal{N}_i \Leftrightarrow i \in \mathcal{N}_j$. Finally, we also denote with $\mathcal{G}(t) = (\mathcal{V}, \mathcal{E}(t))$ the undirected graph induced by this neighboring relationship where the vertices $\mathcal{V}$ represent the agents and $\mathcal{E}(t) = \{(i,j) \in \mathcal{V} \times \mathcal{V} \,|\, \sigma_{ij}(t) = 1 \Leftrightarrow j \in \mathcal{N}_i\}$.

1) Interagent Coupling: We now define the interaction force acting among two neighboring agents. In order to achieve a collision-free, flexible, and cohesive behavior of the fleet, we take inspiration from the interagent coupling proposed in [5] which, in turn, stemmed from the natural behavior of flocks of animals [29]. Let $d_0 < D$ be a desired distance between the agents. If $j \in \mathcal{N}_i$, agent i computes an interaction force F_{ij}^a whose magnitude and direction depend on the relative distance d_{ij} and bearing $\eta_{ij} := (x_i - x_j)/d_{ij}$ between i and j. In particular, the force is always directed along the bearing: If $d_{ij} < d_0$, a repulsive force is generated; if $d_{ij} = d_0$, a null force is produced; and if $d_0 < d_{ij} \leq D$, an attractive force is computed. We also assume that, if $d_{ij} > D$, a null force is generated since, in this case, $j \notin \mathcal{N}_i$ by definition. Notice that, according to the previous definitions, it is $F_{ij}^a = -F_{ji}^a$.

This interagent coupling can be modeled as the gradient of a nonlinear elastic element (virtual spring) that interconnects a pair of agents whenever they are neighbors. A possible potential function $\bar{V}(d_{ij})$ with such a desired behavior is shown in Fig. 2. Note that the shape of the potential goes to infinity as d_{ij} approaches zero for providing an effective interagent repulsive force.[3] As proposed in [30], we then model the elastic coupling between two agents i and j as a (potential) energy storing element

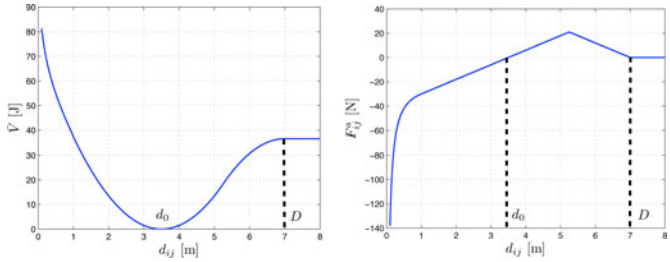

Fig. 2. Shape of the interagent potential as a function of (left) the distance and (right) the corresponding coupling force.

$$\begin{cases} \dot{x}_{ij} = v_{ij} \\ F_{ij}^a = \dfrac{\partial V(x_{ij})}{\partial x_{ij}} \end{cases} \tag{2}$$

where $x_{ij}, v_{ij}, F_{ij}^a \in \mathbb{R}^3$ are, respectively, the state, the input, and the output (i.e., the generated force) of the virtual spring, and $V(x_{ij}) = \bar{V}(\|x_{ij}\|)$ is the spring energy function.

Whenever $j \in \mathcal{N}_i$, the virtual coupling (2) is connected (i.e., exchanges energy) with the dynamics (1) of agents i and j. This formally means that the state x_{ij} is initialized to $x_i - x_j$, $v_{ij} = \dot{x}_i - \dot{x}_j = v_i - v_j$ in (2), and F_{ij}^a contributes to F_i^a in (1) as

$$F_i^a = \sum_{j \in \mathcal{N}_i} F_{ij}^a := \sum_{j \in \mathcal{N}_i} \frac{\partial \bar{V}}{\partial d_{ij}} \frac{\partial d_{ij}}{\partial x_{ij}} = \sum_{j \in \mathcal{N}_i} \frac{\partial \bar{V}}{\partial d_{ij}} \eta_{ij}. \tag{3}$$

Symmetrically, when $j \notin \mathcal{N}_i$, the virtual coupling is disconnected from the agent dynamics, i.e., $v_{ij} = 0$ and F_{ij}^a does not contribute to F_i^a.

Remark 2: We note that the interaction force F_i^a can be computed by agent i in a decentralized way. In fact, the computation is based on the shape of the interagent potential (which is known from the design phase), and on the distance and bearing of agents $j \in \mathcal{N}_i$ with respect to agent i.

In order to write the overall agent/spring dynamics (slave side) in a compact form, define $p = (p_1^T, \ldots, p_N^T)^T \in \mathbb{R}^{3N}$, $B = \text{diag}(B_i) \in \mathbb{R}^{3N \times 3N}$, $x = (x_{12}^T, \ldots, x_{1N}^T, x_{23}^T, \ldots, x_{2N}^T, \ldots, x_{N-1N}^T)^T \in \mathbb{R}^{\frac{3N(N-1)}{2}}$ and $F^e = (F_1^{eT}, \ldots, F_N^{eT})^T \in \mathbb{R}^{3N}$, and let $\mathcal{I}_{\mathcal{G}}(t) \in \mathbb{R}^{N \times \frac{N(N-1)}{2}}$ be the incidence matrix of the graph $\mathcal{G}(t)$ with the edge numbering and orientation induced by the entries of vector x. Notice that $\mathcal{I}_{\mathcal{G}}(t)$ has a constant size despite of the time-varying nature of $\mathcal{G}(t)$. Indeed, $j \notin \mathcal{N}_i$ will result in a column of all zeros for $\mathcal{I}_{\mathcal{G}}(t)$ in correspondence to the edge (i,j). It is then possible to model

[3] In general, any lower bounded potential (e.g., the one proposed in [17]) having similar features would be a suitable choice.

the slave side as a mechanical system described by

$$\begin{cases} \begin{pmatrix} \dot{p} \\ \dot{x} \end{pmatrix} = \left[\begin{pmatrix} 0 & \mathcal{I}(t) \\ -\mathcal{I}^T(t) & 0 \end{pmatrix} - \begin{pmatrix} B & 0 \\ 0 & 0 \end{pmatrix} \right] \begin{pmatrix} \dfrac{\partial H}{\partial p} \\ \dfrac{\partial H}{\partial x} \end{pmatrix} + GF^e \\ v = G^T \begin{pmatrix} \dfrac{\partial H}{\partial p} \\ \dfrac{\partial H}{\partial x} \end{pmatrix} \end{cases} \tag{4}$$

where

$$H = \sum_{i=1}^{N} \mathcal{K}_i + \sum_{i=1}^{N-1} \sum_{j=i+1}^{N} V(x_{ij}) \tag{5}$$

is the total energy of the system, $\mathcal{I}(t) = \mathcal{I}_{\mathcal{G}}(t) \otimes I_3$, and $G = (\,(I_N \otimes I_3)^T \quad 0^T\,)^T$, with I_3 and I_N being the identity matrices of order 3 and N, respectively, 0 representing a null matrix of proper size, and $\otimes$ denoting the Krönecker product.

Proposition 1: Assuming $\mathcal{I}(t) = const$, i.e., no splits and joins are taking place because $\sigma_{ij}(t) \equiv const\, \forall i, \forall j \neq i$, system (4) is passive with respect to the input/output pair $(F^e,\, v)$ with storage function H.

Proof: The potential reported in Fig. 2 is a lower bounded function of the scalar distance among the agents $\|x_{ij}\|$ and, as a consequence, a lower bounded function of x_{ij}. By evaluating the time derivative of the storage function (5) $\dot{H} = \left(\frac{\partial^T H}{\partial p} \quad \frac{\partial^T H}{\partial x}\right) \begin{pmatrix} \dot{p} \\ \dot{x} \end{pmatrix}$ along the system trajectories in (4), and by noting that B is positive definite, it follows that

$$\dot{H} = -\frac{\partial^T H}{\partial p} B \frac{\partial H}{\partial p} + v^T F^e \leq v^T F^e \tag{6}$$

which concludes the proof.

Since (4) is a passive system, its interaction with any passive environment will still preserve passivity. This easily allows us to include in inputs F_i^e in (1) an obstacle avoidance action. Indeed, as usual in applications involving mobile agents in unknown environments, we assume that, when they are detected, obstacles are treated as repulsive potentials, producing a force that vanishes if the robot is far enough and grows as the robot comes closer to the obstacle. Such potentials can also be modeled as virtual springs, i.e., passive systems, and their action is considered to be embedded in the terms F_i^e.

2) Split and Join While Preserving the Slave-Side Passivity: Having established passivity of the slave side with a constant interaction graph topology $\mathcal{G} = \text{const}$, we now analyze the general case of a time-varying $\mathcal{G}(t)$ because of the join and split decisions of Definition 1.

Proposition 2: If two agents i and j split according to Definition 1, then passivity of (4) is preserved.

Proof: If agent i and agent j split, the behavior of the slave side can be described by a subgraph of $\mathcal{G}$, $\mathcal{G}' = (\mathcal{V}', \mathcal{E}')$, where $\mathcal{V}' = \mathcal{V}$ and $\mathcal{E}'$ is obtained by $\mathcal{E}$ by erasing the edge connecting vertex i with vertex j. The behavior of the slave side in case of split can be modeled by replacing, in (4), the incidence matrix $\mathcal{I}$ with a new incidence matrix $\mathcal{I}' = \mathcal{I}_{\mathcal{G}'} \otimes I_3$. The passivity of the system then follows from the same arguments of Proposition 1.

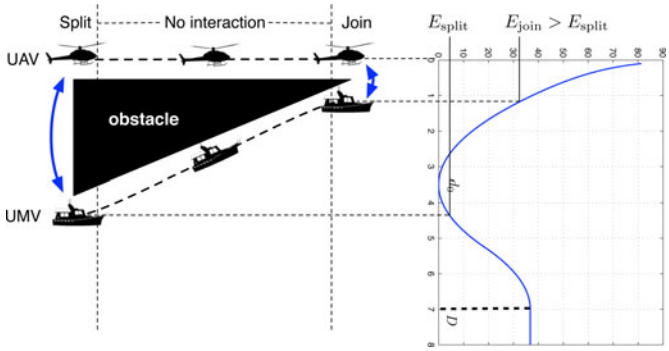

Fig. 3. When the agents (e.g., a UAV and a marine vehicle) split, the energy E_{split} is stored in the spring, while when they join, the energy $E_{\text{join}} > E_{\text{split}}$ is needed to implement the new desired coupling. In this case, without proper strategies, an amount $E_{\text{join}} - E_{\text{split}} > 0$ of energy would be introduced into the system, thus violating passivity.

Remark 3: The fact that passivity of the slave side is preserved despite of changes in $\mathcal{I}$ in (4) due to split decisions depends on the fact that $\mathcal{I}$ enters in the definition of a skew-symmetric matrix which leads to a null term in the energy balance (6). In addition, during a split between two agents i and j, the elastic element x_{ij} becomes isolated from the dynamics of the agents and keeps on storing the same energy $V(x_{ij})$ that was storing before the split decision, while the agents keep on interacting with the rest of the system.

A join decision, on the other hand, can lead to a violation of the slave side passivity: Allowing two agents to join means instantaneously switching from a state characterized by no interaction to the interagent interaction of (2). This results in a new edge in $\mathcal{E}$, and in a corresponding update of the overall incidence matrix $\mathcal{I}$. While, as per Proposition 2, a change in $\mathcal{I}$ does not threaten passivity, some extra energy can still be produced during the join procedure. In fact, in the general case, the relative distance of two agents at the join decision can be different from their relative distance at the split decision, and this can result in a nonpassive behavior as shown in the illustrative example in Fig. 3 where some extra energy is produced when the agents join.

Remark 4: Note that in the particular case of a split because $d_{ij} > D$ followed by a join because $d_{ij} = D$ (see Definition 1), the join decision never threatens passivity: Indeed, when the two agents split, it is $\bar{V}(d_{ij}) = \bar{V}(D)$, and necessarily, when they join, it is again $\bar{V}(d_{ij}) = \bar{V}(D)$. Therefore, no extra energy is produced in this case.

In order to implement the join procedure in a passive way, we then propose to keep track of the energy dissipated by each agent: To this end, we introduce a local variable $t_i \in \mathbb{R}$, which is called *tank*, along with an associated energy function $T_i = \frac{1}{2} t_i^2$ to store the energy dissipated by the agent. This energy reservoir can, then, be used to compensate excess of energy in the slave side and, thus, to implement join decisions without violating the passivity of the system. Using (1), the power dissipated by agent i because of the damping is

$$D_i = p_i^T M_i^{-T} B_i M_i^{-1} p_i. \tag{7}$$

Considering the tank variables, we then adopt the following extended dynamics for the agents and elastic elements:

$$\begin{cases} \dot{p}_i = F_i^a + F_i^e - B_i M_i^{-1} p_i \\ \dot{t}_i = (1-\beta_i)\left(\alpha_i \frac{1}{t_i} D_i + \sum_{j=1\dots N, j\neq i} w_{ij}^T F_{ij}^a\right) + \beta_i c_i \\ y_i = \begin{pmatrix} M_i^{-1} p_i \\ t_i \end{pmatrix} \end{cases} \tag{8}$$

$$\begin{cases} \dot{x}_{ij} = v_{ij} - w_{ij} t_i + w_{ji} t_j \\ F_{ij}^a = \dfrac{\partial V(x_{ij})}{\partial x_{ij}}. \end{cases} \tag{9}$$

The quantity $\alpha_i \in \{0,1\}$ is a design parameter that disables/enables the storage of D_i, the energy dissipated by the system. The quantity $\beta_i \in \{0,1\}$ is a design parameter that allows us to switch the behavior of the tank element from a *storage mode* (i.e., the energy dissipated by the agent is stored) to a *consensus mode* (i.e., a consensus algorithm is run among the tanks). The role of inputs $w_{ij} \in \mathbb{R}^3$ is to allow for an energy exchange among the tank energy T_i and the elastic elements $V(x_{ij})$. Indeed, by setting

$$w_{ij} = \gamma_{ij}(1-\beta_i) t_i F_{ij}^a \tag{10}$$

where $\gamma_{ij} \in \mathbb{R}$ is a modulation parameter, it is possible to implement a *lossless energy transfer* among the storages T_i and $V(x_{ij})$ [8], [31]. In particular, if $\gamma_{ij} > 0$, some energy is extracted from $V(x_{ij})$ and injected into T_i, while the opposite behavior is obtained with $\gamma_{ij} < 0$. The magnitude of γ_{ij} dictates the rate of this exchange, with $\gamma_{ij} = 0$ implying no energy exchange taking place. Note that, while by construction it is $F_{ij}^a = -F_{ji}^a$, in general, $w_{ij} \neq w_{ji}$ and $\gamma_{ij} \neq \gamma_{ji}$. Furthermore, in order to comply with our decentralization guidelines, in (8), we allow for a $\gamma_{ij} \neq 0$ only if $j \in \mathcal{N}_i$. The use of w_{ij} will be illustrated later on.

When the system is in storage mode ($\beta_i = 0$), we have that

$$\dot{T}_i = \alpha_i D_i + t_i \sum_{j\in\mathcal{N}_i} w_{ij}^T F_{ij}^a. \tag{11}$$

If $\alpha_i = 1$ and $\gamma_{ij} = 0$, all the energy dissipated because of the damping injection on the dynamics of agent i is stored back into the tank. This is the energy that can be "used" in the system without violating the passivity constraint. Because of the reasons reported in [32], it is wise to disable the energy storage to avoid an excess of internal energy that would allow us to implement unstable behaviors in the system. Thus, we set

$$\alpha_i = \begin{cases} 0, & \text{if } T_i \geq \bar{T}_i \\ 1, & \text{otherwise} \end{cases} \tag{12}$$

where $\bar{T}_i$ is a proper bound that is to be selected depending on the particular application. In order to avoid singularities in (8) (i.e., $t_i = 0$), we also set a threshold $\varepsilon > 0$ below which it is forbidden to extract energy from the tank.

When the system switches to consensus mode ($\beta_i = 1$), the terms c_i are used to redistribute the energy among the tanks. A decentralized strategy is implemented for equally leveling the energy stored in the tanks just before the join. This is done by running a consensus algorithm [1]

$$\dot{T}_i = -\sum_{j\in\mathcal{N}_i} (T_i - T_j). \tag{13}$$

Such energy redistribution can be implemented acting on the variable t_i. In fact, since $\dot{T}_i = \dot{t}_i t_i$, (13) is equivalent to setting in (8)

$$c_i = -\frac{1}{t_i} \sum_{j\in\mathcal{N}_i} (T_i(t_i) - T_j(t_j)). \tag{14}$$

We will now detail a strategy, which is called `PassiveJoin` procedure, to allow for a safe implementation of join decisions. When agents i and j split, the one with the lower ID between i and j stores x_{ij} in a local variable x_{ij}^s which represents the state of the virtual spring at the split time. If agents i and j never split before, x_{ij}^s is initialized such that $V(x_{ij}^s) = \bar{V}(D) = \bar{V}_{ij}(\infty)$. When two agents i and j want to join, the `PassiveJoin` procedure is preliminary run on agent i (and on agent j with proper modifications on the notation), and the actual join decision (i.e., the update of matrix $\mathcal{I}$) is slightly postponed after its completion. The procedure requires x_{ij}^s (which is shared by the agent with lower ID via local communication) and x_j and t_j that can be sent via local communication by agent j to agent i. First, agent i computes the quantity $\Delta E = V(x_i - x_j) - V(x_{ij}^s)$ (line 1). If $\Delta E \leq 0$, the energy needed to implement the join is lower than the energy previously stored in the spring, and therefore, the join process is actually dissipating energy. Half of the dissipated energy, $(-\Delta E)/2$, can be stored back in the tank of agent i by means of the input w_{ij} (line 3), and the other half will be stored in the tank of the agent j by means of the input w_{ji}. Then, the agents can safely join (line 9).[4]

If $\Delta E > 0$, extra energy is needed to implement the join decision and, at this point, the energy stored in the tanks is exploited. First, the agents check if there is enough energy in their tanks to cover for ΔE (line 4). If this is the case, the amount of energy ΔE_{ij}

$$\Delta E_{ij} = \frac{T(t_i)}{T(t_i) + T(t_j)} \Delta E \tag{15}$$

Procedure PassiveJoin

```
   Data: x_i, x_j, x_ij^s, t_i, t_j
1  Compute ΔE = V(x_i − x_j) − V(x_ij^s);
2  if ΔE ≤ 0 then
3      Store (−ΔE)/2 in the tank through input w_ij;
   else
4      if T_i(t_i) + T_j(t_j) < ΔE + 2ε then
5          Run a consensus on the tank variables;
6          if 2T_i(t_i) < ΔE + 2ε then
7              Dampen until T(t_i) + T(t_j) ≥ ΔE + 2ε;
8      Extract T(t_i)/(T(t_i) + T(t_j)) ΔE from the tank through input w_ij;
9  Join;
```

[4]Formally speaking, the action of inputs w_{ij} and w_{ji} corresponds to moving the state of (9) from x_{ij}^s to the new actual interagent displacement $x_i - x_j$.

is extracted from the tank of agent i by means of the input w_{ij}. At the same time, agent j will extract ΔE_{ji} from its tank using w_{ji} Then, the join is safely implemented (line 9).

If the energy stored in the tanks of the two agents is not sufficient, there is still a chance to passively join the agents without intervening directly on the dynamics of the robots. In fact, it may happen that the tanks of the rest of the fleet, on average, contain enough energy. Thus (line 5), agent i asks the fleet to activate the β_i in order to switch to consensus mode.[5] Then, the consensus is run until the redistribution of the energy among the tanks is completed. Eventually, all the agents switch back to normal mode ($\beta_i = 0$): All the tanks will contain the same amount of energy, but the total tank energy will remain unchanged. After this redistribution, agents i and j check again if there is enough energy in the tanks for joining (line 6). If this is the case, the tank of agent i is updated by means of the input w_{ij} in order to extract the amount of energy in (15) (and symmetrically on agent j), and the join decision is implemented (lines 8 and 9). If, after all, the energy in the tanks is not yet sufficient, it is necessary to act directly on the robots to refill the tanks. This is always possible by augmenting the artificial damping on the agents for increasing the energy dissipation rate. The damping is augmented until $T(t_i) + T(t_j) \geq \Delta E + 2\epsilon$ so that the join decision can be passively implemented extracting the needed amount of energy through the input w_{ij} (lines 7–9).

Remark 5: We assume the convergence time of the consensus to be fast enough compared with the dynamics of the fleet for joining the agents and reestablishing the desired behavior as quickly as possible. In fact, if the algorithm is too slow, the agents may come very close to each other without feeling any repulsive force. If the consensus is not fast enough and some dangerous situation is detected, it can be switched off for dampening the system in order to refill the tanks.

Remark 6: When the damping of the agents is augmented, some time may be needed to refill the tanks up to the desired energy value. During this period, agents i and j can still move because of the interaction with the rest of the group: In this case, their relative distance d_{ij} and the amount of energy necessary to implement the join will change. Therefore, it is necessary to continuously update ΔE when the agents are in damping mode.

The behavior of the slave side when the `PassiveJoin` procedure is implemented can be described by the following system:

$$\begin{cases} \begin{pmatrix} \dot{p} \\ \dot{x} \\ \dot{t} \end{pmatrix} = \left[\begin{pmatrix} 0 & \mathcal{I}(t) & 0 \\ -\mathcal{I}^T(t) & 0 & \Gamma^T \\ 0 & -\Gamma & 0 \end{pmatrix} - \right. \\ \left. - \begin{pmatrix} B & 0 & 0 \\ 0 & 0 & 0 \\ -(I-\beta)\alpha PB & 0 & 0 \end{pmatrix} \right] \begin{pmatrix} \frac{\partial \mathcal{H}}{\partial p} \\ \frac{\partial \mathcal{H}}{\partial x} \\ \frac{\partial \mathcal{H}}{\partial t} \end{pmatrix} + \begin{pmatrix} 0 \\ 0 \\ \beta c \end{pmatrix} + GF^e \\ v = G^T \begin{pmatrix} \frac{\partial \mathcal{H}}{\partial p} \\ \frac{\partial \mathcal{H}}{\partial x} \\ \frac{\partial \mathcal{H}}{\partial t} \end{pmatrix} \end{cases} \tag{16}$$

[5]This can be done by using a decentralized procedure (e.g., the classic flooding algorithm) so that all the agents belonging to the same connected component of the communication graph set $\beta_i = 1$.

where

$$\mathcal{H} = \sum_{i=1}^{N} \mathcal{K}_i + \sum_{i=1}^{N-1} \sum_{j=i+1}^{N} V(x_{ij}) + \sum_{i=1}^{N} T_i \tag{17}$$

is the augmented total energy of the system. The matrix $\Gamma \in \mathbb{R}^{N \times \frac{3N(N-1)}{2}}$ represents the interconnection among tanks and elastic elements mediated by inputs w_{ij}. From (8), one can readily verify that matrix Γ has a structure "equivalent" to the incidence matrix $\mathcal{I}_\mathcal{G}$ with the $(i,\ j)$th element being replaced by the (row) vector w_{ij}^T. Formally, by letting Γ_{ij} and $\mathcal{I}_{\mathcal{G}_{ij}}$ represent the $(i,\ j)$th elements of Γ and $\mathcal{I}_\mathcal{G}$, respectively, it is

$$\Gamma_{i,(3j-2\ldots3j)} = \mathcal{I}_{\mathcal{G}_{ij}} w_{ij}^T, \forall i = 1 \ldots N,\ \forall j = 1 \ldots N(N-1)/2.$$

Finally, $\alpha = \text{diag}(\alpha_i)$ and $\beta = \text{diag}(\beta_i)$ are matrices containing the mode switching parameters, $P = \text{diag}(\frac{1}{t_i} p_i^T M_i^{-T})$, $t = (t_1, \ldots, t_N)^T$, and $c = (c_1, \ldots, c_N)^T$.

Proposition 3: The system represented in (16) is passive with respect to the input/output pair $(F^e,\ v)$ with storage function $\mathcal{H}$.

Proof: By evaluating the time derivative of the storage function

$$\dot{\mathcal{H}} = \begin{pmatrix} \frac{\partial^T \mathcal{H}}{\partial p} & \frac{\partial^T \mathcal{H}}{\partial x} & \frac{\partial^T \mathcal{H}}{\partial t} \end{pmatrix} \begin{pmatrix} \dot{p} \\ \dot{x} \\ \dot{t} \end{pmatrix} \tag{18}$$

along the system trajectories, we obtain

$$\begin{aligned} \dot{\mathcal{H}} &= -\frac{\partial^T \mathcal{H}}{\partial p} B \frac{\partial \mathcal{H}}{\partial p} + \frac{\partial^T \mathcal{H}}{\partial t}(I-\beta)\alpha PB \frac{\partial \mathcal{H}}{\partial p} + \beta \frac{\partial \mathcal{H}}{\partial t} c + v^T F^e \\ &= h_1 + h_2 + h_3 + v^T F^e. \end{aligned} \tag{19}$$

The system is passive if the sum of the first three terms of (19) is lower or equal to 0. The first term h_1 is always nonpositive because B is positive definite. The parameter β can either be equal to the null or identity matrix.

When $\beta = 0$, $h_3 = 0$ and the second term

$$h_2 = \frac{\partial^T \mathcal{H}}{\partial t} \alpha PB \frac{\partial \mathcal{H}}{\partial p} = (\, t_1 \ldots t_N \,)\, \alpha \begin{pmatrix} \frac{1}{t_1} D_1 \\ \vdots \\ \frac{1}{t_N} D_N \end{pmatrix} = \sum_{i=1}^{N} \alpha_i D_i \tag{20}$$

is, because of (12), at most equal to the energy dissipated by the agents, i.e., $-h_1$. Therefore, $\dot{\mathcal{H}} \leq v^T F^e$.

When $\beta = I$, $h_2 = 0$ and the consensus is running among the tanks. By recalling (14), h_3 can be written as

$$h_3 = \frac{\partial^T \mathcal{H}}{\partial t} c = \sum_{i=1}^{N} \dot{T}_i. \tag{21}$$

Because of the property of the consensus, the overall energy stored in the tanks remains the same, and therefore, $h_3 = 0$, and $\dot{\mathcal{H}} \leq v^T F^e$.

Remark 7: Note that, although (16) has a switching dynamics because of the time-varying nature of $\mathcal{I}(t)$ arising from the neighboring conditions $\sigma_{ij}(t)$ of Definition 1, stability issues are avoided thanks to the action of the `PassiveJoin` procedure which prevents positive jumps in $\mathcal{H}$ at any switching time.

B. Master Side

The master can be a generic mechanical system modeled by the following Euler–Lagrange equations:

$$M_M(x_M)\ddot{x}_M + C_M(x_M, \dot{x}_M)\dot{x}_M + D_M\dot{x}_M = F_M \quad (22)$$

where x_M and $\dot{x}_M$ represent the position and the velocity of the end-effector, $M_M(x_M)$ represents the inertia matrix, $C(x_M, \dot{x}_M)\dot{x}_M$ is a term representing the centrifugal and Coriolis effects, D_M is the matrix representing both the viscous friction present in the system and any additional damping injection via local control actions. As often happens for master devices, we also assume that gravity effects are locally compensated. A system described by (22) is passive with respect to the force–velocity pair (F_M, v_M) [33], where $v_M := \dot{x}_M$. This kind of passivity is well suited in standard passivity-based bilateral teleoperation, where the velocity of the master and the velocity of the slave need to be synchronized.

Nevertheless, in our setting, in order to consider the difference between the workspace of the master and that of the robots at the slave side, it is necessary to synchronize the *position* of the master with the *velocity* of the leader. Unfortunately, a mechanical system is not passive with respect to the position–force pair but, following [34], it is possible to render the master (22) passive with respect to the pair (F_M, r) with storage function $V_M = \frac{1}{2} r^T M_M r$ and $r = v_M + \lambda x_M$, $\lambda > 0$. This is obtained by a suitable prefeedback action requiring knowledge of the matrixes M_M and C_M in (22). By further introducing a scaling into this strategy, one can also render the master passive with respect to the scaled pair (F_M, r_M), where

$$r_M = \rho r = \rho v_M + \rho\lambda x_M = \rho v_M + K x_M \quad (23)$$

$\rho > 0$, $\lambda > 0$, and new (scaled) storage function $\bar{V}_M = \rho V_M$. The following result then easily follows.

Proposition 4: A mechanical system that has been made passive with respect to the pair (r, F_M) is also passive with respect to the pair (r_M, F_M).

Proof: Since the system is passive with respect to the pair (r, F_M), it is

$$r^T F_M \geq \dot{V}_M. \quad (24)$$

Using (23), we have that

$$r_M^T F_M = \rho r^T F_M \geq \rho \dot{V}_M = \dot{\bar{V}}_M. \quad (25)$$

Therefore, the system is passive with respect to the lower bounded function $\bar{V}_M$.

Thus, by properly choosing ρ and λ, it is possible to make negligible the contribution related to $\dot{x}_M$ (by choosing a small ρ), and make the second term proportional to the position with a desired scaling factor K (by choosing $\lambda = \frac{K}{\rho}$).

C. Master–Slave Interconnection

Exploiting the results developed so far, we have that both master and slave sides are passive systems. Thus, by designing a proper passive interconnection between the local and the remote systems, we will obtain a passive bilateral teleoperation system characterized by a stable behavior in case of interaction with passive environments (as the obstacles, modeled as potentials, with which the fleet is interacting).

Suppose that agent l is chosen as the leader. It is possible to write $F_l^e = F_s + F_l^{\text{env}}$, where F_l^{env} is the component of the force due to the interaction with the external environment (obstacles), and F_s is the component due to the interaction with the master side. Similarly, we can decompose F_M as $F_M = F_m + F_h$, where F_h is the component due to the interaction with the user, and F_m is the force acting on the master because of the interaction with the slave.

For achieving the desired teleoperation behavior, we propose to join master and slave using the following interconnection:

$$\begin{cases} F_s = b_T(r_M - v_l) \\ F_m = -b_T(r_M - v_l) \end{cases}, \quad b_T > 0. \quad (26)$$

This is equivalent to joining the master and the leader using a damper which generates a force proportional to the difference of the two velocity-like variables of the master and the leader. Since r_M is "almost" the position of the master, we have that the force fed back to the master and the control action sent to the leader are the desired ones. The overall teleoperation system is represented in Fig. 1 and consists of the interconnection of a passive master side, a damper-like interconnection, and a passive slave side. By letting $\bar{F}^e = (\, F_1^{e^T} \;\; \cdots \;\; F_l^{env^T} \;\; \cdots \;\; F_N^{e^T} \,)^T$ be the vector of the forces due to the interaction with the external environment, the following proposition holds.

Proposition 5: The teleoperation system composed of the precompensated master side presented in Section II-B, the slave side reported in (16), and the interconnection (26) is passive with respect to the pair $((\bar{F}^e)^T, F_h^T)^T, (v^T, r_M^T)^T$.

Proof: Considering the decomposition of F_M and of F_l^e, from Proposition 3 and from (25), we can state that

$$\begin{cases} v^T F^e = v^T \bar{F}^e + v_l^T F_s \geq \dot{\mathcal{H}} \\ r_M^T F_h + r_M^T F_m \geq \dot{\bar{V}}_M. \end{cases} \quad (27)$$

Since (26) implies

$$v_l^T F_s + r_M^T F_m = -b_T(r_M - v_l)^T(r_M - v_l) \leq 0 \quad (28)$$

by taking $\mathcal{H}_{\text{tot}} = \mathcal{H} + \bar{V}_M$ as lower bounded storage function, and by exploiting (27) and (28), it follows that

$$v^T \bar{F}^e + r_M^T F_h \geq \dot{\mathcal{H}}_{\text{tot}} + b_T(r_M - v_l)^T(r_M - v_l) \geq \dot{\mathcal{H}}_{\text{tot}}. \quad (29)$$

This proves passivity of the master/slave interconnection.

It is also straightforward to passively consider communication delays between local and remote sites using one of the techniques developed for single-master single-slave systems, like, for example, the two-layer approach [35]. This way, the system would keep on exhibiting a stable behavior independently of any delay between local and remote sites.[6]

III. Steady-State Analysis

Without loss of generality, we assume, in this section, that agent $l = 1$ is the leader, implying that $F_1^e = F_1^{\text{env}} + F_s$ and

[6]We assume that negligible delays are present within the slave side because of the spatial proximity of the agents.

$F_i^e = F_i^{\text{env}}$ for $i = 2, \ldots, N$. The goal of the following analysis is to characterize the steady-state behavior of the overall teleoperation system in two relevant regimes: free-motion (i.e., $F_i^{\text{env}} = 0, \forall i = 1, \ldots, N$) and hard contact with obstacles (i.e., $v_i = 0, \forall i = 1, \ldots, N$, despite $r_M \neq 0$).

A. Steady State During Free Motion

We first consider the free-motion case and denote with $\mathcal{G}_{\mathcal{L}}$ the connected component of $\mathcal{G}$ containing the leader. In this situation, we assume that 1) the agents are sufficiently far away from any obstacle so that $F_i^{\text{env}} = 0, \forall i$, 2) there exists a certain time $\bar{\tau}$ after which no splits and joins take place in $\mathcal{G}_{\mathcal{L}}$ and tanks are fully charged at their maximum value $\bar{T}_i$, and 3) the master device is kept at a constant position $\bar{x}_M \equiv$ const by a suitable human force F_h whose steady-state value will be determined in the following.

The following proposition shows that, under these assumptions, the robots belonging to $\mathcal{G}_{\mathcal{L}}$ reach a steady-state regime in which all the agents possess the same velocity $v_{ss} \in \mathbb{R}^3$ as a function of $\bar{x}_M$. In addition, it also indicates the steady-state value of the force F_h exerted by the human operator to keep the master device at $\bar{x}_M$. We start introducing the following preliminary definitions. We assume that $\mathcal{G}_{\mathcal{L}}$ contains $1 \leq N_{\mathcal{L}} \leq N$ agents whose indexes are collected into the set $\mathcal{L}$ so that $|\mathcal{L}| = N_{\mathcal{L}}$. Note that $1 \in \mathcal{L}$ by construction. We then let $p_{\mathcal{L}} \in \mathbb{R}^{3N_{\mathcal{L}}}$, $x_{\mathcal{L}} \in \mathbb{R}^{\frac{3N_{\mathcal{L}}(N_{\mathcal{L}}-1)}{2}}$, and $t_{\mathcal{L}} \in \mathbb{R}^{N_{\mathcal{L}}}$ represent the entries of p, x, and t associated with this component, and $p_{\bar{\mathcal{L}}} \in \mathbb{R}^{3(N-N_{\mathcal{L}})}$, $x_{\bar{\mathcal{L}}} \in \mathbb{R}^{\frac{3(N-N_{\mathcal{L}})(N-N_{\mathcal{L}}-1)}{2}}$, and $t_{\bar{\mathcal{L}}} \in \mathbb{R}^{N-N_{\mathcal{L}}}$ the remaining ones, where $\bar{\mathcal{L}}$ denotes the complement of $\mathcal{L}$. Accordingly, we let $\mathcal{H}_{\mathcal{L}}$ and $\mathcal{H}_{\bar{\mathcal{L}}}$ be the components of the total energy $\mathcal{H}$ depending on $(p_{\mathcal{L}}, x_{\mathcal{L}}, t_{\mathcal{L}})$ and $(p_{\bar{\mathcal{L}}}, x_{\bar{\mathcal{L}}}, t_{\bar{\mathcal{L}}})$, respectively. Furthermore, we let $\mathbf{1}_{N_{\mathcal{L}3}} = \mathbf{1}_{N_{\mathcal{L}}} \otimes I_3$, with $\mathbf{1}_{N_{\mathcal{L}}} \in \mathbb{R}^{N_{\mathcal{L}}}$ being a column vector of all ones, and $B_{\mathcal{L}} \in \mathbb{R}^{3N_{\mathcal{L}} \times 3N_{\mathcal{L}}} = \text{diag}(B_{\mathcal{L}_i})$, with $B_{\mathcal{L}_1} = B_1 + b_T I_3$ and $B_{\mathcal{L}_i} = B_i$, $i \in \mathcal{L}$, $i \neq 1$. Finally, we define, with v_{ss} and F_{ss}, the (sought) steady-state values for the agents in $\mathcal{L}$ and for the force exerted by the human operator.

Proposition 6: (Steady State in Free Motion): Under assumptions 1–3, the system (16) reaches a steady state characterized by $(\dot{p}, \dot{x}, \dot{t}) = (0, 0, 0)$ in which

1) every robot belonging to $\bar{\mathcal{L}}$ comes to a full stop;
2) every robot belonging to $\mathcal{L}$ has the same velocity $v_{ss} = (\mathbf{1}_{N_{\mathcal{L}3}}^T B_{\mathcal{L}} \mathbf{1}_{N_{\mathcal{L}3}})^{-1} b_T K \bar{x}_m$;
3) the human operator needs to apply a force $F_h = (I_3 - b_T (\mathbf{1}_{N_{\mathcal{L}3}}^T B_{\mathcal{L}} \mathbf{1}_{N_{\mathcal{L}3}})^{-1}) b_T K \bar{x}_m$ to keep the master device at $\bar{x}_M$.

Proof: We start by noting that, $\forall\, x_{ij}$ not included in $x_{\mathcal{L}}$ and $x_{\bar{\mathcal{L}}}$, $\dot{x}_{ij} = 0$ as it necessarily represents the state of a disconnected virtual spring. Furthermore, the subsystem $(p_{\bar{\mathcal{L}}}, x_{\bar{\mathcal{L}}}, t_{\bar{\mathcal{L}}})$ not belonging to $\mathcal{L}$ is governed by the dynamics

$$\begin{pmatrix} \dot{p}_{\bar{\mathcal{L}}} \\ \dot{x}_{\bar{\mathcal{L}}} \\ \dot{t}_{\bar{\mathcal{L}}} \end{pmatrix} = \begin{pmatrix} -B_{\bar{\mathcal{L}}} & \mathcal{I}_{\bar{\mathcal{L}}} & 0 \\ -\mathcal{I}_{\bar{\mathcal{L}}}^T & 0 & 0 \\ 0 & 0 & 0 \end{pmatrix} \begin{pmatrix} \frac{\partial \mathcal{H}_{\bar{\mathcal{L}}}}{\partial p_{\bar{\mathcal{L}}}} \\ \frac{\partial \mathcal{H}_{\bar{\mathcal{L}}}}{\partial x_{\bar{\mathcal{L}}}} \\ \frac{\partial \mathcal{H}_{\bar{\mathcal{L}}}}{\partial t_{\bar{\mathcal{L}}}} \end{pmatrix} \tag{30}$$

for some $\mathcal{I}_{\bar{\mathcal{L}}}$ and positive definite $B_{\bar{\mathcal{L}}}$ of proper dimensions. Since the tanks are supposed to be full (assumption 2), no energy exchange takes place among tanks and elastic elements, and $\dot{t}_{\bar{\mathcal{L}}} = 0$. Therefore, by evaluating the rate of change of $\mathcal{H}_{\bar{\mathcal{L}}}$ along (30), one obtains

$$\dot{\mathcal{H}}_{\bar{\mathcal{L}}} = -\frac{\partial^T \mathcal{H}_{\bar{\mathcal{L}}}}{\partial p_{\bar{\mathcal{L}}}} B_{\bar{\mathcal{L}}} \frac{\partial \mathcal{H}_{\bar{\mathcal{L}}}}{\partial p_{\bar{\mathcal{L}}}} \leq 0$$

i.e., the system is output strictly passive, implying that the system will converge toward the condition $\frac{\partial \mathcal{H}_{\bar{\mathcal{L}}}}{\partial p_{\bar{\mathcal{L}}}} = v_{\bar{\mathcal{L}}} \equiv 0 \Rightarrow p_{\bar{\mathcal{L}}} \equiv 0 \Rightarrow \dot{p}_{\bar{\mathcal{L}}} \equiv 0$. From the second row of (30), this further implies that $\dot{x}_{\bar{\mathcal{L}}} \equiv 0$, resulting in a steady state $(\dot{p}_{\bar{\mathcal{L}}}, \dot{x}_{\bar{\mathcal{L}}}, \dot{t}_{\bar{\mathcal{L}}}) = (0, 0, 0)$ where all the agents in $\bar{\mathcal{L}}$ eventually reach a full stop ($v_{\bar{\mathcal{L}}} = 0$). This proves item 1) of the Proposition.

Coming to items 2) and 3), note that, because of assumption 3, we have $\dot{x}_M = \ddot{x}_M \equiv 0$ and $r_M = K \bar{x}_M$. By splitting F_s into the two components $b_T K \bar{x}_M$ and $-b_T v_1$, the subsystem $(p_{\mathcal{L}}, x_{\mathcal{L}}, t_{\mathcal{L}})$ belonging to $\mathcal{L}$ becomes

$$\begin{cases} \begin{pmatrix} \dot{p}_{\mathcal{L}} \\ \dot{x}_{\mathcal{L}} \\ \dot{t}_{\mathcal{L}} \end{pmatrix} = \begin{pmatrix} -B_{\mathcal{L}} & \mathcal{I}_{\mathcal{L}} & 0 \\ -\mathcal{I}_{\mathcal{L}}^T & 0 & 0 \\ 0 & 0 & 0 \end{pmatrix} \begin{pmatrix} \frac{\partial \mathcal{H}_{\mathcal{L}}}{\partial p_{\mathcal{L}}} \\ \frac{\partial \mathcal{H}_{\mathcal{L}}}{\partial x_{\mathcal{L}}} \\ \frac{\partial \mathcal{H}_{\mathcal{L}}}{\partial t_{\mathcal{L}}} \end{pmatrix} + \begin{pmatrix} u \\ 0 \end{pmatrix} \\ v_{\mathcal{L}} = G^T \begin{pmatrix} \frac{\partial \mathcal{H}_{\mathcal{L}}}{\partial p_{\mathcal{L}}} \\ \frac{\partial \mathcal{H}_{\mathcal{L}}}{\partial x_{\mathcal{L}}} \\ \frac{\partial \mathcal{H}_{\mathcal{L}}}{\partial t_{\mathcal{L}}} \end{pmatrix} \end{cases} \tag{31}$$

where $\mathcal{I}_{\mathcal{L}} = (\mathcal{I}_{\mathcal{G}_{\mathcal{L}}} \otimes I_3)$, $\mathcal{I}_{\mathcal{G}_{\mathcal{L}}}$ being the incidence matrix associated with $\mathcal{G}_{\mathcal{L}}$, and $u \in \mathbb{R}^{3N_{\mathcal{L}}}$ is a constant vector whose first three entries are $b_T K \bar{x}_M$ and the remaining ones are zero. In order to draw conclusions on the asymptotical (steady state) behavior of (31) when excited with a constant u, we resort to the arguments illustrated in [36, Prop 8.1.1]. To this end, consider the constant input u as being generated by the following neutrally stable exosystem:

$$\begin{cases} \dot{\omega} = 0 \\ u = \omega. \end{cases} \tag{32}$$

Note also that, since system (31) is again output strictly passive, when $u = 0$, one obtains

$$\dot{\mathcal{H}}_{\mathcal{L}} = -\frac{\partial^T \mathcal{H}_{\mathcal{L}}}{\partial p_{\mathcal{L}}} B_{\mathcal{L}} \frac{\partial \mathcal{H}_{\mathcal{L}}}{\partial p_{\mathcal{L}}} \leq 0$$

yielding an asymptotically stable equilibrium point corresponding to a (local) minimum of its energy. Therefore, the assumptions required by Proposition 8.1.1 are met and system (31) admits a steady-state regime. This is characterized by a map $\pi(\cdot)$

$$\pi : \omega \mapsto \begin{pmatrix} p_{\mathcal{L}} \\ x_{\mathcal{L}} \end{pmatrix}, \quad \pi(\omega) = \begin{pmatrix} \pi_1(\omega) \\ \pi_2(\omega) \end{pmatrix} \tag{33}$$

satisfying the following condition:

$$0 = \begin{pmatrix} -B_{\mathcal{L}} & \mathcal{I}_{\mathcal{L}} \\ -\mathcal{I}_{\mathcal{L}}^T & 0 \end{pmatrix} \begin{pmatrix} M_{\mathcal{L}}^{-1} \pi_1(\omega) \\ \nu(\pi_2(\omega)) \end{pmatrix} + \begin{pmatrix} \omega \\ 0 \end{pmatrix} \tag{34}$$

where $\nu(\cdot) := \frac{\partial \mathcal{H}}{\partial x}(\cdot)$ and $M_{\mathcal{L}}$ is the inertia matrix associated with the agents in $\mathcal{L}$. Now, rewrite (34) as

$$B_{\mathcal{L}} M_{\mathcal{L}}^{-1} \pi_1(\omega) - \mathcal{I}_{\mathcal{L}} \nu(\pi_2(\omega)) = \omega \tag{35}$$

$$\mathcal{I}_{\mathcal{L}}^T M_{\mathcal{L}}^{-1} \pi_1(\omega) = 0. \tag{36}$$

As the group of agents that we are considering is connected, it is well known that $\mathrm{rank}(\mathcal{I}_{\mathcal{G}_\mathcal{L}}^T) = N_\mathcal{L} - 1$ and $\ker(\mathcal{I}_{\mathcal{G}_\mathcal{L}}^T) = \mathbf{1}_{N_\mathcal{L}}$ (see, e.g., [19]). Then, from (36), it follows that

$$M_\mathcal{L}^{-1}\pi_1(\omega) = \mathbf{1}_{N_{\mathcal{L}3}} v_{ss} \tag{37}$$

for a certain $v_{ss} \in \mathbb{R}^3$. Plugging (37) into (35), we obtain

$$\mathcal{I}_\mathcal{L}\nu(\pi_2(\omega)) = B_\mathcal{L}\mathbf{1}_{N_{\mathcal{L}3}} v_{ss} - \omega. \tag{38}$$

This is a linear equation in the unknowns $\nu(\pi_2(\omega))$ and it admits a solution iff the right-hand side (RHS) belongs to $\mathrm{Im}(\mathcal{I}_\mathcal{L})$. Since, from standard linear algebra, $\mathrm{Im}(\mathcal{I}_\mathcal{L}) = \ker(\mathcal{I}_\mathcal{L}^T)^\perp = \mathrm{span}(\mathbf{1}_{N_{\mathcal{L}3}})^\perp$, the RHS of (38) must satisfy

$$\mathbf{1}_{N_{\mathcal{L}3}}^T(B_\mathcal{L}\mathbf{1}_{N_{\mathcal{L}3}} v_{ss} - \omega) = 0.$$

This condition yields the sought value for the steady-state agent velocities

$$v_{ss} = (\mathbf{1}_{N_{\mathcal{L}3}}^T B_\mathcal{L}\mathbf{1}_{N_{\mathcal{L}3}})^{-1}\mathbf{1}_{N_{\mathcal{L}3}}^T\omega = (\mathbf{1}_{N_{\mathcal{L}3}}^T B_\mathcal{L}\mathbf{1}_{N_{\mathcal{L}3}})^{-1} b_T K\bar{x}_M. \tag{39}$$

Therefore, by taking v_{ss} as in (39), it is always possible to solve (38) for some $\nu(\pi_2(\omega))$ whose specific value is, however, not required for this analysis. Thus, the steady state for system (31) is given by

$$\begin{pmatrix} p_{\mathcal{L}ss} \\ x_{\mathcal{L}ss} \end{pmatrix} := \pi(\omega) = \begin{pmatrix} M_\mathcal{L}\mathbf{1}_{N_{\mathcal{L}3}} v_{ss} \\ \nu(\pi_2(\omega)) \end{pmatrix} = \text{const} \tag{40}$$

as $\omega = \text{const}$ by definition. Furthermore, expanding (40), for each agent $i \in \mathcal{L}$ at steady state, it is $v_i = M_i^{-1}p_i = M_i^{-1}M_i v_{ss} = v_{ss}$, i.e., all the agents in $\mathcal{L}$ will reach the same steady-state velocity v_{ss}, proving item 2).

Finally, noting that (22) and the assumption 3) $\ddot{x}_M = \dot{x}_M = 0$ imply $0 = F_M = F_m + F_h$, we have, at steady state

$$\begin{aligned} F_h = -F_m = F_{ss} &:= b_T(K\bar{x}_M - v_{ss}) = \\ &= (I_3 - b_T(\mathbf{1}_{N_{\mathcal{L}3}}^T B_\mathcal{L}\mathbf{1}_{N_{\mathcal{L}3}})^{-1})b_T K\bar{x}_M \end{aligned} \tag{41}$$

which proves item 3) and concludes the proof.

Remark 8: Note that (39) is always well posed because $B_\mathcal{L}$ is a positive-definite matrix. In the particular case of damping terms taking the form $B_i = b_i I_3$, $b_i > 0$, (39) reduces to

$$v_{ss} = \frac{b_T K\bar{x}_M}{b_T + \sum_{i\in\mathcal{L}} b_i} \tag{42}$$

and (41) becomes

$$F_{ss} = \frac{b_T K\bar{x}_M \sum_{i\in\mathcal{L}} b_i}{b_T + \sum_{i\in\mathcal{L}} b_i}. \tag{43}$$

It is easy to check that, as $\left(\sum_{i\in\mathcal{L}} b_i\right)/b_T \to 0$ (small b_i, large b_T), $v_{ss} \to K\bar{x}_M = r_M$ and $F_{ss} \to 0$, thus approaching perfect synchronization with the commanded velocity r_M. The same, however, holds for the more general forms (39) and (41) as well.

At steady state, the human operator needs to apply a force $F_h = F_{ss}$ proportional to the commanded velocity $K\bar{x}_M$ by a factor which depends on the number of agents $N_\mathcal{L}$ belonging to the connected component of the leader $\mathcal{L}$, and on the magnitude of their damping terms in B_i. For a given $\mathcal{L}$, force F_h will mimic a spring centered on a zero velocity command [see (41)–(43)]. Thus, if the number of agents in $\mathcal{L}$ is constant, this force cue will increase/decrease proportionally to the steady-state absolute speed of the whole group: This can provide a haptic cue informative of the overall group velocity.

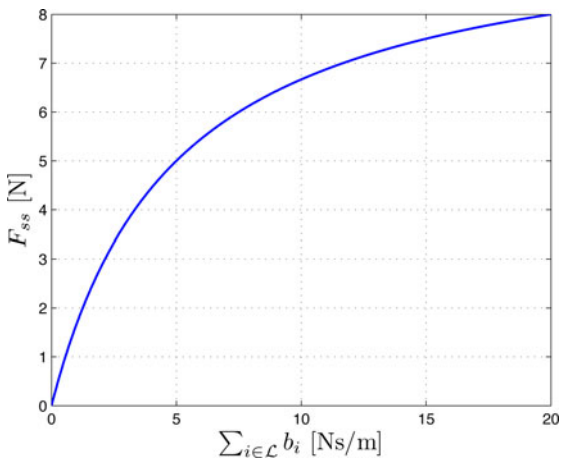

Fig. 4. Steady-state force F_{ss} during free motion as a function of the total damping of the agents belonging to $\mathcal{L}$. Note how F_{ss} increases with the number of agents $N_\mathcal{L}$ belonging to $\mathcal{L}$.

On the other hand, for a given *fixed* commanded velocity $K\bar{x}_M$, F_h will still vary with the size of $\mathcal{L}$ because of the term $\sum_{i\in\mathcal{L}} b_i$ in (43). Fig. 4 shows an illustrative behavior of F_h in this case with $\bar{x}_M \equiv 2$, $K = 1$, and $b_T = 5$. One can then check that the force F_h needed to keep a constant velocity $K\bar{x}_M$ increases with the size of $N_\mathcal{L}$. This behavior can also be intuitively explained by considering the followers as a passive environment the leader is interacting with. In fact, it is known from standard bilateral teleoperation (see, e.g., [37]) that in this case, perfect steady-state "synchronization" between master and slave velocities cannot be achieved resulting in a residual nonnull steady-state force.

However, we believe that this behavior can constitute a beneficial feature of our teleoperation design. In fact, the force F_h resulting from such master/slave velocity mismatch can provide the user with an additional information about the status of the group. Consider the illustrative example where the operator is moving the whole fleet with a constant cruise speed by firmly keeping the master device at a certain constant position $\bar{x}_M$. By virtue of (41), whenever a robot disconnects from the group $\mathcal{L}$, the human operator would feel a decrease in the force needed to keep the master device at x_M. This negative slope in F_h can be informative of the fact that the number of robots in the connected component of leader has decreased. Similarly, when a robot connects to the group, the user would feel a positive slope in F_h, thus informing him/her about the increased number of robots in $\mathcal{L}$.

B. Steady State During Hard Contact With Obstacles

We now proceed to analyze the hard contact situation corresponding to the case where, in addition to assumptions 2 and 3, we also assume that 4) $\frac{\partial\mathcal{H}_\mathcal{L}}{\partial p_\mathcal{L}} =: v_\mathcal{L} \equiv 0$ despite $r_M \neq 0$ (e.g., because the obstacles are obstructing the agent motion).

Proposition 7: (Hard Contact With Obstacles): Under the assumptions 2–4, the system (16) reaches a steady state characterized by $(\dot{p},\, \dot{x},\, \dot{t}) = (0,\, 0,\, 0)$ in which

1) every robot belonging to $\bar{\mathcal{L}}$ comes to a full stop;
2) there is a perfect force reflection on the human operator of the cumulative environmental forces stopping the robots belonging to $\mathcal{L}$, i.e., $F_h = -\sum_{i\in\mathcal{L}} F_i^{\text{env}}$.

Proof: Proof of item 1) follows from the same arguments used in Proposition 6. Because of assumption 4 ($v_{\mathcal{L}} = 0$), the first row of (31) reduces to

$$0 = \mathcal{I}_{\mathcal{L}} \frac{\partial \mathcal{H}_{\mathcal{L}}}{\partial x_{\mathcal{L}}} + u \tag{44}$$

where now $u \in \mathbb{R}^{3N_{\mathcal{L}}} = (\dots\ u_i^T\ \dots)$, $i \in \mathcal{L}$, with $u_1 = F_s + F_1^{\text{env}}$ and $u_i = F_i^{\text{env}}$, $i \neq 1$. By left multiplying (44) with $\mathbf{1}_{N_{\mathcal{L}3}}^T$, and by exploiting again the fact that $\ker(\mathcal{I}_{\mathcal{L}}) = \text{span}(\mathbf{1}_{N_{\mathcal{L}3}})$, we get $\mathbf{1}_{N_{\mathcal{L}3}}^T u = 0$ that can be expanded as $F_s = -\sum_{i\in\mathcal{L}} F_i^{\text{env}}$. Furthermore, because of assumption 3, it is again $0 = F_M = F_h + F_m$ and, by using (26), we finally obtain

$$F_h = -F_m = F_s = -\sum_{i\in\mathcal{L}} F_i^{\text{env}}.$$

This proves item 2) and concludes the proof.

IV. Simulation and Experimental Results

In this section, we will report the results of several HHL simulations and experiments conducted to validate the theoretical framework developed so far. A picture representing our testbed is shown in Fig. 5. The master side consists of a 3-DOF force-feedback device, the Omega.3[7] [see Fig. 5(c)], controlled via USB by a C++ program running on a dedicated GNU-Linux machine. This includes two threads: The first thread runs a synchronous loop at 2.5 kHz which accesses the current master position/velocity and sets the control force F_m in (26). The second thread, which is running at a slower rate triggered by the leader control rate (60 Hz in the simulation case and 120 Hz for the experiments), acts as a network interface with the leader agent by exchanging the leader speed v_l and the master command r_M. By using the standard interface provided by the manufacturer, we are able to apply a 3-D Cartesian force to the end-effector and to automatically compensate for gravity terms.

In order to illustrate the flexibility of our method, we conducted several HHL simulations with a slave side consisting of a heterogeneous group of robots including both quadrotor UAVs and differentially driven ground robots (UGVs). All the robots are physically simulated within a custom-made environment based on the Ogre3D engine for 3-D rendering and computational geometry calculations, and PhysX to simulate the physical interaction between the mobile robots and the environment[8] [see Fig. 5(a), (b), and (d)]. Note that both class of mobile robots meet the assumption of Remark 1. In particular, we relied on a cascaded controller for the UAV Cartesian motion and on a proportional-integral-derivative (PID) controller for the attitude

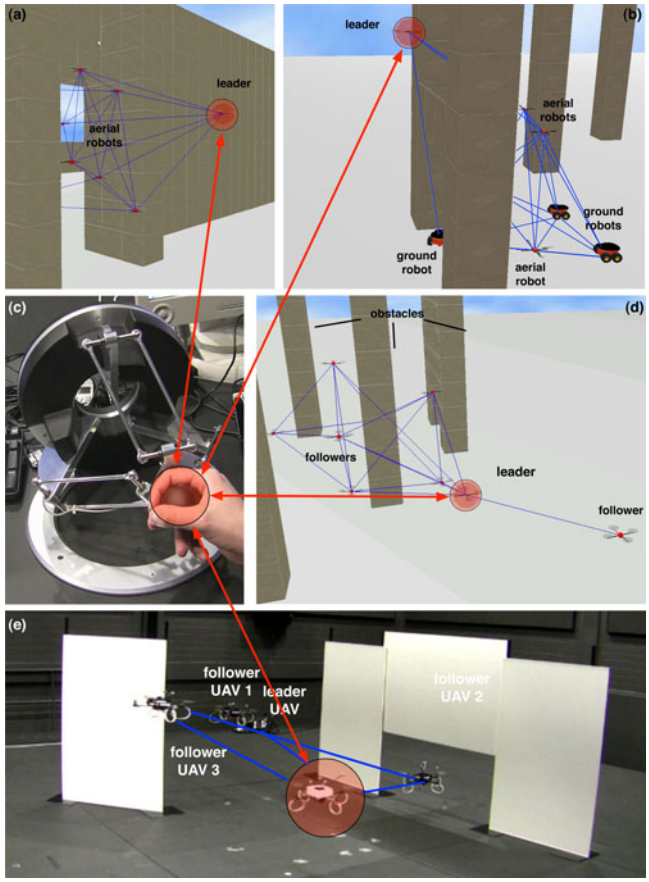

Fig. 5. HHL simulative and experimental setup. (a), (b), and (d): Three screenshots of a physically based simulation in a cluttered environment involving a fleet of (a) and (d) either eight quadrotors or (b) five quadrotors and three differentially driven ground robots (b). The leader is highlighted by a transparent red ball; inter-agent visibility and distance are considered as neighboring criteria; neighbor agents are linked by blue lines. (c) Omega-3 force-feedback master device handled by the human operator. (e) Screenshot of an experiment with four real quadrotors in a cluttered environment where the leader is highlighted by a transparent red ball.

(i.e., pitch and roll) and yaw-rate DOFs. As for the UGVs, we employed a standard trajectory controller based on feedback linearization. Each mobile-robot (UAV/UGV) trajectory controller runs, in a decentralized way, as a separate process. This design facilitates the porting of the whole implementation on real hardware. Every process is in charge of 1) communicating with the other mobile robots, 2) communicating with the master device (only the process controlling the leader), 3) implementing the interagent behavior described in Section II-A, 4) retrieving the current UAV/UGV state and the surrounding obstacle points from the simulator, and 5) implementing the trajectory tracking controller mentioned in Remark 1. All the communication is implemented with the user datagram protocol (UDP) since it is less prone to congestions and delay issues compared with the transmission control protocol.

In the experiments, the slave side is composed of four quadrotors[9] equipped with an embedded ATmega microcontroller and a standard integrated IMU [see Fig. 5(e)]. The

[7]http://www.forcedimension.com
[8]http://www.ogre3d.org/, http://www.nvidia.com/object/physx_new.html
[9]http://www.mikrokopter.com

microcontroller implements a low-level PID attitude controller by estimating the current attitude from the IMU measurements (via a complementary filter), and by controlling the pitch, roll, thrust, and yaw-rate DOFs of the UAV. This PID controller runs at about 450 Hz. Every quadrotor is also equipped with an additional Qseven single-board GNU-Linux machine running a C++ program which implements a higher level Cartesian-control module: This computes the desired attitude and thrust commands and sends them to the low-level microprocessor via a serial interface whose baud rate is set to 115 200. As opposed to the simulation case, the Qseven board 1) retrieves the current UAV position (and numerically estimates its velocity) from an external tracking system and 2) receives the obstacle positions from the simulation environment where the physical obstacles are simulated in parallel. All the ethernet communication is again implemented with the UDP protocol.

In all simulations and experiments, we simulated the presence of a visibility sensor to retrieve the position of neighboring agents. Therefore, compatibly with the requirements of Definition 1, we also set $\sigma_{ij} = 0$ whenever the line of sight between agents i and j was occluded. The agents were then forced to split either because of too large interdistances ($d_{ij} > D$), or because of occlusions on their line of sights, an event which can also occur when $d_{ij} < D$. Of course, different choices for deciding splits are possible, but they are equivalent with respect to the conceptual behavior of the `PassiveJoin` procedure. We also assumed without loss of generality that the leader is agent 1. The reader is encouraged to watch the video clip attached to the paper where both simulations and experiments in cluttered environments with frequent split and join decisions can be fully appreciated.

A. Simulation Results

In the first HHL simulation, which is reported in Fig. 6(a)–(e), we tested the overall performance of the teleoperation scheme during free-motion (i.e., sufficiently away from obstacles). The goal was to validate the claims of Proposition 6 about stability and steady-state characteristics of our teleoperation system. We considered a leader and seven followers, and teleoperated the leader with (almost) piecewise constant velocity commands r_M, as shown in Fig. 6(a). During the simulation, we kept all the 7 agents within the connected component containing the leader $\mathcal{L}$, and chose $b_T = 4.5$ [N·s/m], $B_1 = 1I_3$ [N·s/m], $B_i = 2.3I_3$ [N·s/m] for $i = 2, \ldots, 8$, and $K = 15$ [1/s].

Fig. 6(b) shows the superimposition of the actual leader velocity v_1 (dashed lines) and the predicted steady-state velocity v_{ss} (solid lines): As clear from the plot, when r_M is kept constant, v_1 converges to v_{ss} after short transients due to the interaction with the rest of the group. This is also evident from Fig. 6(c), where the superimposition of the velocities of all the agents (leader included) is shown: One can, then, verify that all the UAV/UGV velocities converge to the same steady-state value v_{ss}. In order to quantify this convergence, we show, in Fig. 6(d), the norm of $e_v = v - \mathbf{1}_{N_3} v_{ss}$, i.e., the velocity error of the overall slave side with respect to the steady-state value v_{ss}. As expected, $\|e_v\|$ goes to zero whenever the master command r_M is kept constant.

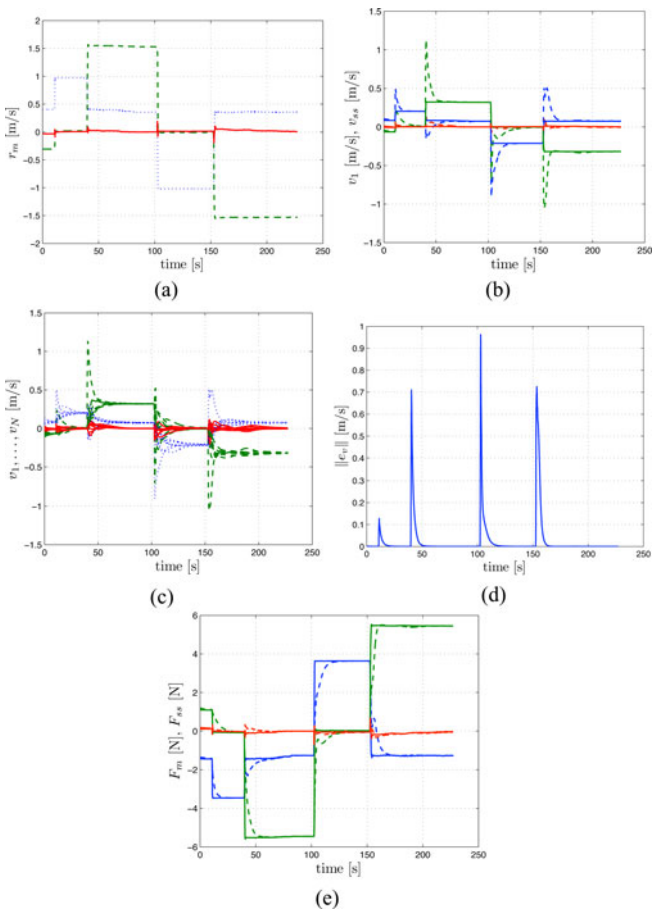

Fig. 6. Results of the first HHL simulation. (a) Velocity command $r_M(t)$ set by the human operator (three components, x solid blue, y dashed green, and z dotted red). (b) Superimposition of $v_1(t)$ (the leader velocity in dashed lines) and $v_{ss}(t)$ (the predicted steady-state velocity in solid lines). (c) Superimposition of the velocities of all the agents (three components, x solid blue, y dashed green, and z dotted red). (d) Behavior of $\|e_v\|$, the norm of the velocity error of every agent with respect to the predicted v_{ss}. (e) Superimposition of the force $F_m(t)$ applied to the master because of the interaction with the slave (dashed lines) and its predicted steady-state value F_{ss} (solid lines).

Finally, Fig. 6(e) reports the behavior of F_m over time: One can note that F_m (dashed lines) converges to the predicted steady-state value of Proposition 6 (solid lines). As explained in the previous section, this force cue is useful to inform the operator about the absolute velocity and total number of agents being teleoperated.

In the second HHL simulation, we report the teleoperation of eight mobile robots (one leader and seven followers) moving in an environment cluttered with obstacles, thus enabling the possibility of several split and rejoin decisions. We set $\bar{T}_i = 8$ [J] as the maximum value for the tank energies T_i. Fig. 7(a) shows the evolution of the eight reservoirs T_i from which one can appreciate the several negative jumps due to the execution of the `PassiveJoin` procedure. We also show, in Fig. 7(b) and (c), a detailed view of the tank evolutions during a few consecutive consensus phases in which the tank energies are quickly leveled. Finally, Fig. 7(d) shows the behavior of $E_{\text{ext}}(t) = \int_{t_0}^{t} v^T(\tau) F^e(\tau) \mathrm{d}\tau$ (blue line) and $E_{\text{in}}(t) = \mathcal{H}(t) - \mathcal{H}(t_0)$ (dashed red line) over time. One can,

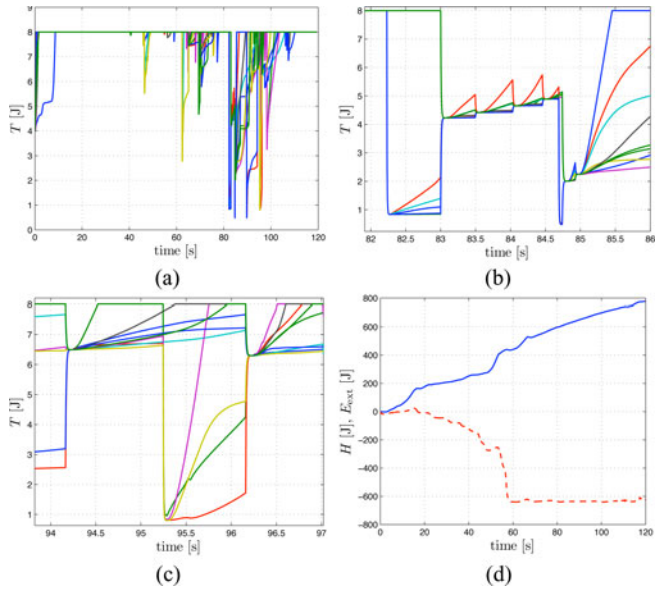

Fig. 7. Results of the second HHL simulation. (a) Behavior of $T(t)$ over time during several split and join decisions. Negative jumps in $T(t)$ correspond to energy exchanges between tanks and link potentials in order to ensure passivity of the slave side (`PassiveJoin` Procedure). (b) and (c) Zoomed view of the tank energies during consecutive consensus phases. d) Behavior of $E_{\rm ext}(t)$ (blue line) and $E_{\rm in}(t)$ (red line), validating the slave side passivity condition (19) also during the split/join decisions.

then, check that $E_{\rm in}(t) \leq E_{\rm ext}(t)$, $\forall t \geq t_0$, as required by the slave-side passivity condition (19).

B. Experimental Results

Experiments have been carried on with a team of four quadrotors in the environment depicted in Fig. 8(e). The results of a representative experiment are shown in Fig. 8. The velocity command $r_M(t)$ set by the human operator is depicted in Fig. 8(c), while Fig. 8(a) illustrates the behavior of the positions x_1 of the leader agent with dynamics (1) (three solid lines) and the corresponding real positions $x_{1,\rm real}$ of the associated quadrotor (three dashed line). As can be noticed, the dashed lines are basically indistinguishable from the solid lines, indicating that the robot could track the "virtual" position of (1) with a negligible error. Similarly, Fig. 8(b) shows the behavior of $\|e_x\|$ over time, that is the average norm of the position error $x_i - x_{i,\rm real}$, $i = 1, \ldots, 4$: This plot confirms again that the overall tracking performance of the four quadrotors with respect to their simplified dynamics (1) was quite satisfactory as this error norm stays small during the whole operation.

Fig. 8(e) shows the force-feedback signal applied to the haptic device computed from (26): Here, the largest peaks correspond to the largest mismatches between the commanded and actual leader velocity due to the interaction with the followers and the obstacles. Fig. 8(d) reports the behavior of the tank energies over time during several split and join decisions. Negative jumps in $T_i(t)$ correspond to energy exchanges between tanks and link potentials in order to ensure passivity of the slave side (see again the `PassiveJoin` procedure). Finally, Fig. 8(f) validates the slave-side passivity condition (19), also during the experiments,

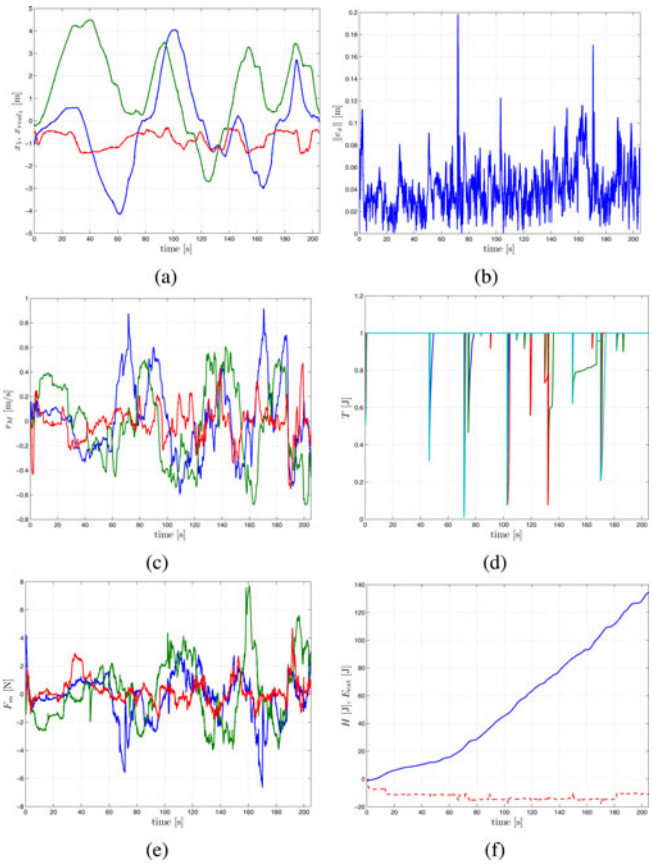

Fig. 8. Results of a representative experiment. (a) Behavior of the three components of the positions x_1 of the leader agent (solid line) and $x_{1,\rm real}$ of the associated robot (dashed line)—note how they almost perfectly overlap. b) Behavior of $\|e_x\|$, which is the average norm of the tracking errors $x_i - x_{i,\rm real}$: Note how this quantity keeps very small over time, indicating an overall good tracking performance of the quadrotors with respect to the assumed dynamics (1). (c) Velocity command $r_M(t)$ set by the human operator (three components: x blue, y green, and z red). d) Behavior of the tank energies $T(t)$ over time during several split and join decisions. e) Components of the 3-D force $F_m(t)$ applied to the master because of the interaction with the slave. (f) Behavior of $E_{\rm ext}t)$ (blue line) and $E_{\rm in}(t)$ (red line).

by showing that the energy provided to the system $E_{\rm ext}(t)$ (blue line) is always lower bounded by $E_{\rm in}(t) = \mathcal{H}(t) - \mathcal{H}(t_0)$ (red line).

Fig. 9 depicts four different screenshots of the experiment (the leader robot, agent 1, is encircled by a red ball). The human operator action is shown in the left column, while the central column shows the motion of the group and the right column gives a corresponding top-view from a 3-D visualizer. The edges of the interaction graph are represented by blue links: One can appreciate the time-varying nature of the interaction topology since the interconnection graph changes depending on the relative position between robots and because of occlusions by the obstacles. At the beginning (first row), the interaction graph is a chain, while at the end (fourth row) it is a clique (complete graph). The two middle rows show again two different graph topologies resulted during the teloperation of the robots. Note how the group is able to seamlessly adapt to the cluttered nature of the environment thanks to its varying interaction topology.

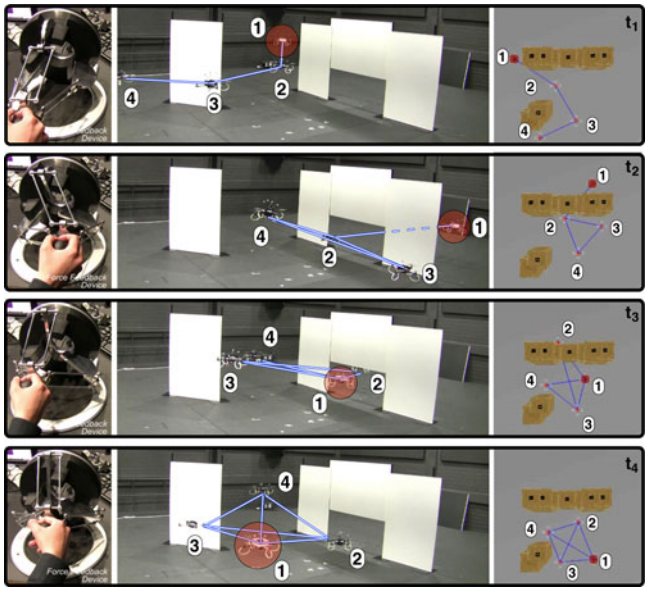

Fig. 9. Each row denotes a different moment of a representative experiment. The left column shows the human operator commanding the leader robot with a 3-DOF haptic device. The central column represents four UAVs in an environment with obstacles (the white walls with a narrow passage). The right column shows the corresponding top view in a 3-D visualizer. The time-varying interaction graph is enlightened by the presence of blue links representing its edges.

V. Conclusion and Future Work

In this paper, we have proposed a decentralized control strategy based on passivity for teleoperating a team of, possibly heterogeneous, mobile robots. By monitoring the exchange of energy among the robots, we were able to obtain a flexible behavior of the group that could smoothly modify the shape of its formation and the communication topology in a stable way. By properly passifying the master robot, a passive bilateral teleoperation system that couples the position of the master to the velocity of the slave side has been developed. The steady-state free motion and contact behaviors of the teleoperation system have been analytically characterized. Finally, the performance of the system has been validated through HHL simulations and real experiments considering a group of UAVs as case study.

In recent works, we considered the issue of connectivity maintenance in the case of distance-visibility neighboring conditions (see [38]), and of decentralized velocity synchronization thanks to a suitable variable damping actions; see [39]. We also started to run an extended psychophysical evaluation to study the human perceptual awareness and maneuverability in the teleoperation of a group of mobile robots [40], [41]. As additional extensions of this framework, we are considering the possibility to allow the presence of variable multiple leaders to increase the controllability of the fleet. In the future, we also plan to explicitly take into account interrobot communication delays to formally study the corresponding teleoperation stability issues, and to change online the elasticity of the couplings among the followers in order to adapt the behavior of the group to particular environments or tasks.

Acknowledgment

The authors would like to thank M. Ryll and J. Lächele for their assistance in the experimental testbed and the setup of the simulator, respectively.

References

[1] R. M. Murray, "Recent research in cooperative control of multi-vehicle systems," *ASME J. Dyn. Syst., Meas., Control*, vol. 129, no. 5, pp. 571–583, 2007.

[2] A. Howard, L. E. Parker, and G. S. Sukhatme, "Experiments with a large heterogeneous mobile robot team: Exploration, mapping, deployment and detection," *Int. J. Robot. Res.*, vol. 25, no. 5–6, pp. 431–447, 2006.

[3] M. Schwager, D. Rus, and J. J. Slotine, "Decentralized adaptive coverage control for networked robots," *Int. J. Robot. Res.*, vol. 28, no. 3, pp. 357–375, 2009.

[4] J. Fink, N. Michael, S. Kim, and V. Kumar, "Planning and control for cooperative manipulation and transportation with aerial robots," *Int. J. Robot. Res.*, vol. 30, no. 3, pp. 324–334, 2011.

[5] N. E. Leonard and E. Fiorelli, "Virtual leaders, artificial potentials and coordinated control of groups," in *Proc. 40th IEEE Conf. Decis. Control*, Orlando, FL, Dec. 2001, pp. 2968–2973.

[6] N. Guenard, T. Hamel, and L. Eck, "Control laws for the tele operation of an unmanned aerial vehicle known as an X4-flyer," in *Proc. IEEE/RSJ Int. Conf. Intell. Robots Syst.*, Beijing, China, Oct. 2006, pp. 3249–3254.

[7] R. Mahony, F. Schill, P. Corke, and Y. S. Oh, "A new framework for force feedback teleoperation of robotic vehicles based on optical flow," in *Proc. IEEE Int. Conf. Robot. Autom.*, Kobe, Japan, May 2009, pp. 1079–1085.

[8] S. Stramigioli, R. Mahony, and P. Corke, "A novel approach to haptic tele-operation of aerial robot vehicles," in *Proc. IEEE Int. Conf. Robot. Autom.*, Anchorage, AK, May 2010, pp. 5302–5308.

[9] B. Hannaford, "Stability and performance tradeoffs in bi-lateral telemanipulation," in *Proc. IEEE Int. Conf. Robot. Autom.*, Scottsdale, AZ, May1989, pp. 1764–1767.

[10] B. Hannaford, L. Wood, D. A. McAffee, and H. Zak, "Performance evaluation of a six-axis generalized force-reflecting teleoperator," *IEEE Trans. Syst., Man, Cybern.*, vol. 21, no. 3, pp. 620–633, May/Jun. 1991.

[11] T. M. Lam, H. W. Boschloo, M. Mulder, and M. M. V. Paassen, "Artificial force field for haptic feedback in UAV teleoperation," *IEEE Trans. Syst., Man, Cybern. A: Syst. Humans*, vol. 39, no. 6, pp. 1316–1330, Nov. 2009.

[12] D. A. Abbink, M. Mulder, F. C. T. van der Helm, M. Mulder, and E. R. Boer, "Measuring neuromuscular control dynamics during car following with continuous haptic feedback," *IEEE Trans. Syst., Man, Cybern. B: Cybern.*, vol. 41, no. 5, pp. 1239–1249, Oct. 2011.

[13] S. Sirouspour, "Modeling and control of cooperative teleoperation systems," *IEEE Trans. Robot.*, vol. 21, no. 6, pp. 1220–1225, Dec. 2005.

[14] D. Lee and M. W. Spong, "Bilateral teleoperation of multiple cooperative robots over delayed communication network: Theory," in *Proc. IEEE Int. Conf. Robot. Autom.*, Barcelona, Spain, Apr. 2005, pp. 360–365.

[15] D. Lee, "Semi-autonomous teleoperation of multiple wheeled mobile robots over the internet," presented at the ASME Dyn. Syst. Control Conf., Ann Arbor, MI, Oct. 2008.

[16] Y. Cheung and J. S. Chung, "Cooperative control of a multi-arm system using semi-autonomous telemanipulation and adaptive impedance," presented at the 14th Int. Conf. Robot., Munich, Germany, Jun. 2009.

[17] E. J. Rodríguez-Seda, J. J. Troy, C. A. Erignac, P. Murray, D. M. Stipanović, and M. W. Spong, "Bilateral teleoperation of multiple mobile agents: Coordinated motion and collision avoidance," *IEEE Trans. Control Syst. Technol.*, vol. 18, no. 4, pp. 984–992, Jul. 2010.

[18] D. Lee, A. Franchi, P. R. Giordano, H. I. Son, and H. H. Bülthoff, "Haptic teleoperation of multiple unmanned aerial vehicles over the internet," in *Proc. IEEE Int. Conf. Robot. Autom.*, Shanghai, China, May 2011, pp. 1341–1347.

[19] M. Mesbahi and M. Egerstedt, *Graph Theoretic Methods in Multiagent Network*, (Princeton Series in Applied Mathematics), 1st ed. Princeton, NJ: Princeton Univ. Press, 2010.

[20] H. G. Tanner, A. Jadbabaie, and G. J. Pappas, "Flocking in fixed and switching networks," *IEEE Trans. Autom. Control*, vol. 52, no. 5, pp. 863–868, May 2007.

[21] P. F. Hokayem and M. W. Spong, "Bilateral teleoperation: An historical survey," *Automatica*, vol. 42, no. 12, pp. 2035–2057, 2006.

[22] A. Franchi, P. R. Giordano, C. Secchi, H. I. Son, and H. H. Bülthoff, "A passivity-based decentralized approach for the bilateral teleoperation of a

group of UAVs with switching topology," in *Proc. IEEE Int. Conf. Robot. Autom.*, Shanghai, China, May 2011, pp. 898–905.
[23] E. Nuño, L. Basañez, and R. Ortega, "Passivity-based control for bilateral teleoperation: A tutorial," *Automatica*, vol. 47, no. 3, pp. 485–495, 2011.
[24] A. Franchi, H. H. Bülthoff, and P. R. Giordano, "Distributed online leader selection in the bilateral teleoperation of multiple UAVs," in *Proc. 50th IEEE Conf. Decis. Control*, Orlando, FL, Dec. 2011, pp. 3559–3565.
[25] M. Fliess, J. Lévine, P. Martin, and P. Rouchon, "Flatness and defect of nonlinear systems: Introductory theory and examples," *Int. J. Control*, vol. 61, no. 6, pp. 1327–1361, 1995.
[26] R. M. Murray, M. Rathinam, and W. Sluis, "Differential flatness of mechanical control systems: A catalog of prototype systems," presented at the ASME Int. Mech. Eng. Congr. Expo., San Francisco, CA, Nov. 1995.
[27] S. Bouabdallah and R. Siegwart, "Backstepping and sliding-mode techniques applied to an indoor micro," in *Proc. IEEE Int. Conf. Robot. Autom.*, May 2005, pp. 2247–2252.
[28] N. Michael and V. Kumar, "Planning and control of ensembles of robots with non-holonomic constraints," *Int. J. Robot. Res.*, vol. 28, no. 8, pp. 962–975, 2009.
[29] I. D. Couzin, "Collective minds," *Nature*, vol. 445, p. 715, 2007. Available: http://www.nature.com/nature/journal/v445/n7129/full/445715a.html.
[30] C. Secchi and C. Fantuzzi, "Formation control over delayed communication networks," in *Proc. IEEE Int. Conf. Robot. Autom.*, Pasadena, CA, May 2008, pp. 563–568.
[31] C. Secchi, S. Stramigioli, and C. Fantuzzi, "Position drift compensation in port-Hamiltonian based telemanipulation," in *Proc. IEEE/RSJ Int. Conf. Intell. Robots Syst.*, Beijing, China, Oct. 2006, pp. 4211–4216.
[32] D. J. Lee and K. Huang, "Passive-set-position-modulation framework for interactive robotic systems," *IEEE Trans. Robot.*, vol. 26, no. 2, pp. 354–369, Apr. 2010.
[33] C. Secchi, S. Stramigioli, and C. Fantuzzi, *Control of Interactive Robotic Interfaces: A port-Hamiltonian Approach* (Tracts in Advanced Robotics Series). New York: Springer-Verlag, 2007.
[34] N. Chopra, M. W. Spong, and R. Lozano, "Synchronization of bilateral teleoperators with time delay," *Automatica*, vol. 44, no. 8, pp. 2142–2148, 2008.
[35] C. Secchi, A. Franchi, H. H. Bülthoff, and P. R. Giordano, "Bilateral teleoperation of a group of UAVs with communication delays and switching topology," presented at the IEEE Conf. Robot. Autom., St. Paul, MN, May 2012.
[36] A. Isidori, *Nonlinear Control Systems*, 3rd ed. New York: Springer-Verlag, 1995.
[37] G. Niemeyer and J. J. Slotine, "Telemanipulation with time delays," *Int. J. Robot. Res.*, vol. 23, no. 9, pp. 873–890, 2004.
[38] P. R. Giordano, A. Franchi, C. Secchi, and H. H. Bülthoff, "Passivity-based decentralized connectivity maintenance in the bilateral teleoperation of multiple UAVs," presented at the 2011 Robot.: Sci. Syst. Conf., Los Angeles, CA, Jun. 2011.
[39] P. R. Giordano, A. Franchi, C. Secchi, and H. H. Bülthoff, "Experiments of passivity-based bilateral aerial teleoperation of a group of UAVs with decentralized velocity synchronization," in *Proc. IEEE/RSJ Int. Conf. Intell. Robots Syst.*, San Francisco, CA, Sep. 2011, pp. 163–170.
[40] H. I. Son, J. Kim, L. Chuang, A. Franchi, P. R. Giordano, D. Lee, and H. H. Bülthoff, "An evaluation of haptic cues on the tele-operator's perceptual awareness of multiple UAVs' environments," in *Proc. IEEE World Haptics Conf.*, Istanbul, Turkey, Jun. 2011, pp. 149–154.
[41] H. I. Son, L. L. Chuang, A. Franchi, J. Kim, D. J. Lee, S. W. Lee, H. H. Bülthoff, and P. R. Giordano, "Measuring an operator's maneuverability performance in the haptic teleoperation of multiple robots," in *Proc. IEEE/RSJ Int. Conf. Intell. Robots Syst.*, San Francisco, CA, Sep. 2011, pp. 3039–3046.

Antonio Franchi (S'07–M'11) received the Laurea degree (*summa cum laude*) in electronic engineering and the Ph.D. degree in control and system theory from the Sapienza University of Rome, Rome, Italy, in 2005 and 2009, respectively.

Since 2010, he has been a Research Scientist with the Max Planck Institute for Biological Cybernetics, Tübingen, Germany. He was a visiting student with the University of California, Santa Barbara, in 2009. His main research interests include control of autonomous systems and robotics, including planning, cooperative control, estimation, haptics, and human–machine interaction.

Cristian Secchi (M'04) received the Laurea degree in computer science engineering, from the University of Bologna, Bologna, Italy, in 2000 and the Ph.D. degree in information engineering from the University of Modena and Reggio Emilia, Reggio Emilia, Italy, in 2004.

He is currently an Assistant Professor with the University of Modena and Reggio Emilia. His main research interests include teleoperation, mobile robotics, and the control of mechatronic systems.

Dr. Secchi was an Associate Editor of the *IEEE Robotics and Automation Magazine* from 2006 to 2008 and has been the Co-Chair of the IEEE Robotics and Automation Society Technical Committee on telerobotics since 2007.

Hyoung Il Son (M'11) received the B.S. and M.S. degrees from the Department of Mechanical Engineering, Pusan National University, Busan, Korea, in 1998 and 2000, respectively, and the Ph.D. degree from the Department of Mechanical Engineering, Korea Advanced Institute of Science and Technology, Daejeon, Korea in 2010.

Since 2010, he has been a Research Scientist with the Max Planck Institute for Biological Cybernetics, Tübingen, Germany. He was a Senior Researcher with LG Electronics from 2003 to 2005 and Samsung Electronics from 2005 to 2009. He was a Research Associate with the University of Tokyo, Tokyo, Japan, in 2010. His research interests include haptics, teleoperation, psychophysics-based control design and evaluation, and supervisory control of discrete event/hybrid systems.

Heinrich H. Bülthoff (M'96) received the Ph.D. degree in natural sciences from Eberhard Karls University, Tübingen, Germany, where he received the Ph.D. degree in biology in 1980.

From 1980 to 1988 he was a Research Scientist with the Max Planck Institute (MPI) for Biological Cybernetics, Tübingen, and the Massachusetts Institute of Technology, Cambridge. From 1988 to 1993, he was an Assistant, Associate, and Full Professor of cognitive science with Brown University, Providence, RI. He became the Director of the Department for Human Perception, Cognition and Action, MPI for Biological Cybernetics, and a scientific member of the Max Planck Society in 1993. Since 1996, he has been a Honorary Professor with Eberhard Karls University as well as an Adjunct Professor with Korea University, Seoul, Korea. His research interests include object recognition and categorization, perception and action in virtual environments, and human–robot interaction and perception.

Paolo Robuffo Giordano (M'08) received the M.Sc. degree in computer science engineering and the Ph.D. degree in systems engineering from the Sapienza University of Rome, Rome, Italy, in 2001 and 2008, respectively.

From 2007 to 2008, he spent one year as a Postdoctoral Researcher with the Institute of Robotics and Mechatronics, German Aerospace Center. In 2008, he joined the Max Planck Institute for Biological Cybernetics, Tübingen, Germany, where he is currently a Senior Research Scientist Head of the Human–Robot Interaction Group. His research interests include nonlinear control, robotics, haptics, and virtual reality applications.